



TECHNISCHE
UNIVERSITÄT
WIEN

Master's thesis

Development of a New Method for Determination of Ash Behavior in Fluidized Bed Conversion Processes

A thesis submitted for the master's degree in Chemical and Process Engineering

supervised by

Univ.Prof. Dipl.-Ing. Dr.techn. Hermann Hofbauer

co-supervised by

DI Dr.techn. Matthias Kuba

at the Institute of Chemical, Environmental and Bioscience Engineering

E 166

at TU Wien

by

Juraj Priscak, BSc

Matriculation number: 01329449

Bystricka 25

841 07 Bratislava

Vienna, February 2020

Juraj Priscak

Acknowledgements

I would like to express my profound gratitude to Prof. Hermann Hofbauer for the opportunity to work on this interesting topic in his research group of Gasification and Gas Cleaning at TU Wien. I am also very grateful to my co-supervisor Dr. Matthias Kuba for his permanent support and for the scientific guidance.

I would like to thank all the colleagues from BEST - Bioenergy and Sustainable Technologies GmbH as well as from TU Wien for all the support I have received during last years.

Finally, I wish to express my gratitude to my family and friends for their constant support, especially to my mother Maria and my wife Miška.

Ďakujem!

Abstract

Within a fluidized bed reactor, bed material particles interact with the fuel ash at elevated temperatures. As a consequence of these interactions operational problems such as sintering and agglomeration can occur, which causes changes in fluidization dynamics. Although it can be in some cases beneficial (e.g. fluidized bed granulation) in the case of fluidized bed conversion processes agglomeration is an undesired phenomenon which causes significant operating problems and in the worst case scenario can cause total defluidization of the bed. Therefore the understanding of the ash behavior during thermochemical conversion processes (gasification and combustion), as well as creating of a reliable method for the prediction of the ash melting in the fluidized bed reactor is necessary. Several methods such as the ash fusion test, the compression- strength- based test or the controlled fluidization bed agglomeration test can be used to determine the ash melting temperature in the fluidized bed. However these tests takes into account neither the influence of the local overheating caused by burning char particles nor progressive accumulation of ash in the bed. That can be problematic in the case of fuels like wheat straw lignin or rice husk, where formation and accumulation of coherent ash particles at the top of the bed leads to serious operational problems.

The aim of this master's thesis is therefore to develop a realistic and reliable method for determination of ash problematic behavior within the fluidized bed reactor during thermochemical conversion processes. Unlike presently used techniques this one should also take into account the influence of the local overheating caused by burning char particles and progressive accumulation of ash in the bed.

Table of contents

Acknowledgements	i
Abstract	ii
Table of contents	iii
1. Introduction	1
1.1. Motivation	1
1.2. Aim of this work	2
2. Fundamentals	3
2.1. Biomass.....	3
2.1.1. Definition of biomass.....	3
2.1.2. Biomass resources	3
2.2. Thermochemical conversion of biomass	4
2.2.1. Pyrolysis.....	4
2.2.2. Gasification	4
2.2.2.1. Gasification process	5
2.2.2.2. Dual Fluidized Bed Steam Gasification.....	6
2.2.3. Combustion.....	7
2.3. Ash chemistry	7
2.3.1. Ash transformation chemistry.....	7
2.3.2. Reactions of alkali metals with other species during thermochemical conversion processes	10
2.4. Agglomeration	11
2.4.1. Agglomeration mechanisms.....	11
2.4.2. Melt-induced agglomeration.....	12
2.4.3. Coating-induced agglomeration	12
2.5. Layer formation.....	13
2.5.1. Quartz	13
2.5.2. Olivine	15
2.6. Methods of agglomeration determination	17
2.6.1. The ASTM ash fusion test method.....	17
2.6.2. The Sintering Test Method.....	17
2.6.3. The Controlled Fluidized Bed Agglomeration Method.....	18

2.6.4. Comparison of the methods.....	18
3. Materials and Methods.....	20
3.1. Fuel and bed material preparation.....	20
3.1.1. Fuel preparation.....	20
3.1.2. Fuel analysis.....	21
3.1.3. Bed material preparation.....	23
3.2. Descriptions of the fluidized bed reactors.....	23
3.2.1. Lab-scale fluidized bed reactor.....	24
3.2.2. Bench-scale reactor.....	25
3.2.3. 100kW DFB pilot-plant.....	26
3.3. Developed method for determination of ash behavior in FB conversion processes.....	28
3.3.1. Experiments in the lab-scale reactor.....	28
3.3.2. Experiments in the bench-scale reactor.....	28
3.4. Behavior of lignin ash in a steady-state operation in 100kW DFB pilot-plant.....	29
3.5. Equilibrium calculations in Factsage.....	29
4. Results.....	31
4.1. Lab-scale FB reactor.....	31
4.1.1. Wheat straw.....	31
4.1.2. Lignin.....	33
4.2. Bench-scale FB reactor.....	35
4.2.1. Wheat straw.....	35
4.2.2. Lignin.....	37
4.3. 100kW DFB pilot-plant.....	39
4.4. Equilibrium calculations in FactSage 7.2.....	42
4.4.1. Wheat straw.....	42
4.4.2. Lignin.....	46
5. Discussion.....	49
5.1. Wheat straw.....	49
5.2. Lignin.....	51
5.3. Suitability of the reactors for agglomeration tests.....	53
5.4. Comparison of methods for determination of ash behavior in FB reactor....	54
6. Conclusion.....	55

References	57
List of Figures	59
List of Tables	61

Die approbierte gedruckte Originalversion dieser Diplomarbeit ist an der TU Wien Bibliothek verfügbar.
The approved original version of this thesis is available in print at TU Wien Bibliothek.



1. Introduction

1.1. Motivation

The predicted average annual change of the world energy consumption in the next 15 years is 1.5% [1]. In order to meet this increasing demand for energy and also to minimize the air and nature pollution connected to its production, we have to focus more on replacing the fossil fuels by renewable energy sources. Already today, renewable energy resources like wind, sun, and water show great potential to compensate a relevant share of fossil fuels as a primary energy source. The most widespread of the renewable energy resources is biomass, which covers more than 10% of the world primary energy consumption (Figure 1). Using biomass for energy supply is environmental friendly, since biomass can be classified as a CO₂-neutral source.

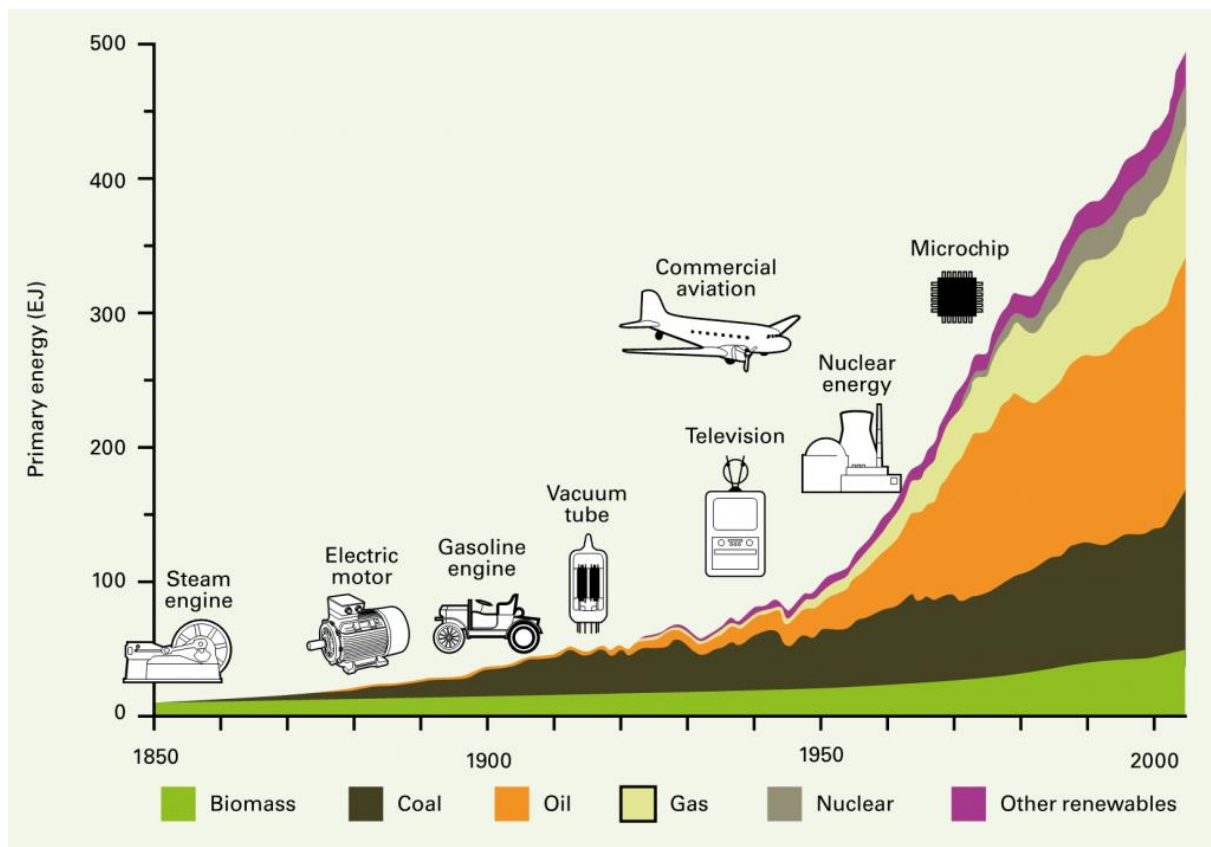


Figure 1: Primary energy consumption increase since 1850 [1]

Especially biomass gasification technology gained more focus in the last years, since in comparison to combustion it converts the solid feedstock into a gaseous product with a useful chemical energy, which can be either used to produce electricity directly in a gas engine, or it can be converted by synthesis processes into biofuels (e.g. Fischer-Tropsch Diesel) and valuable chemicals (e.g. H_2 , CH_4 , bio-alcohols).

The suitability of woody biomass for the gasification process has already been demonstrated in Güssing, Austria [2]. However in lower-rank biomass (e.g. crops and agriculture residues), the ash-forming matter differs from the one in the woody biomass and can cause operational problems such as sintering, agglomeration or eventually total defluidisation of the fluidized bed. These problems are common for both – combustion and gasification reactors [3]. Hence, the understanding of the ash behavior, as well as the creating a reliable method for prediction of problematic ash behavior in the fluidized bed is necessary.

1.2. Aim of this work

The aim of this work is to develop a reliable method for determination of problematic ash behavior such as bed agglomeration during fluidized bed conversion processes. The method should take into account the ash-bed material particle interaction as well as the influence of the local overheating caused by the burning char particles and should be applicable in reducing and oxidizing atmosphere.

The experiments will be performed in a lab-scale (combustion), bench-scale (combustion) and pilot-scale (gasification) reactor. Wheat straw and wheat straw lignin will be used as a feedstock and their agglomeration temperature determined. The results will be compared with those from the ASTM fusion tests and from chemical equilibrium calculations and a suitability of the performed method will be discussed.

2. Fundamentals

2.1. Biomass

2.1.1. Definition of biomass

Generally, biomass refers to any organic matter with a vegetable or an animal origin. According to the United Nations Framework Convention on Climate Change (UNFCCC) [4], biomass can be defined as follows:

“Biomass means non-fossilized and biodegradable organic material originating from plants, animals and micro-organisms. This shall also include products, by-products, residues and waste from agriculture, forestry and related industries as well as the non-fossilized and biodegradable organic fractions of industrial and municipal wastes. Biomass also includes gases and liquids recovered from the decomposition of non-fossilized and biodegradable organic material.”

However, the biomass definition doesn't include any fossil fuel – an organic material that has been formed millions years ago and stored beneath the earth's surface, such as coal, natural gas or petroleum. Unlike fossil fuels, which contribute additional CO₂ into the atmosphere, biomass is considered to be CO₂ neutral, since it recycles only atmospheric carbon.

2.1.2. Biomass resources

Based on their origin, biomass resources can be divided into 3 major groups [5]:

1. biogenic wastes
2. standing forests
3. energy crops

Wastes include agricultural production and processing wastes, crop residues, the mill wood residues, the urban wood wastes and the urban organic wastes. Wood, wood residues, logging residues and forest residues (such as sawdust and bark from forest cleaning) belongs to the second group. The third group -energy crops, is expected to be the largest source of biomass in the future [6]. This category includes short-rotation woody crops, herbaceous woody crops, grasses, starch crops (corn, wheat,

barley), sugar crops (cane and beet), forage crops and oilseed crops (sunflower, soybean, safflower) [5].

2.2. Thermochemical conversion of biomass

Thermochemical conversion of biomass includes three processes: pyrolysis, gasification and combustion.

2.2.1. Pyrolysis

During pyrolysis, biomass is converted into liquid bio-oil, solid charcoal and gases. The process is carried out in absence of oxygen. One of the advantages of pyrolysis is the fact, that it can be adjusted for production of either charcoal or bio-oil up to 95.5% [5]. There are two types of pyrolysis – conventional (or “slow”) and fast pyrolysis. The main product of conventional pyrolysis is solid charcoal and the process temperature is held around 500 °C. The heating rate is much lower compared to the fast pyrolysis and the vapor residence time reaches 30 min. On the other side, the residence time of fast pyrolysis varies between 0.5-5 sec and heating rates reach 1000 °C/s. After reaching 425-500 °C, pyrolysis vapors are rapidly cooled down (quenched). The result of such rapid heating up and cooling down is a liquid product (bio-oil), since higher-molecular-weight species don't have sufficient time to react with each other and break down [7].

2.2.2. Gasification

Gasification is an endothermic chemical process that converts solid carbonaceous fuel into gaseous products. Unlike combustion, where carbon is fully converted into its final oxidation state CO_2 , the product gas (product of gasification) has still useful heating value. Integration of gasification process in an integrated gasification combined cycle (IGCC), where the exhaust heat from the gas turbine is utilized in a steam cycle can achieve overall efficiency of 63.8% [8].

2.2.2.1. Gasification process

The first step of the gasification process is drying. The moisture content of fresh wood can vary in most cases between 30 to 60%. Such high water content considerably decreases the overall efficiency of the process, since the evaporation of water within reactor consumes approximate 2260 kJ/kg of the energy. Hence, in order to increase the process efficiency, the water content of biomass is in most cases decreased to 10-20% with a pre-drying step. The final drying (dehydration) takes place in the gasifier, where remaining water is released from biomass during temperature increase (up to 125 °C) [8]. As the temperature increases further, hydrocarbons within the biomass begin to decompose into smaller molecules. This step is known as pyrolysis, or thermal degradation. Unlike gasification, pyrolysis doesn't require any external agent such as steam, air, oxygen or carbon dioxide. Pyrolysis produces permanent gases, solid chars and liquid tars, which can cause large amount of problems in industrial process. Tars are condensable hydrocarbons which condensate at lower temperatures, forming a highly viscous liquid that tends to clog gas lines downstream the gasifier. Gasification takes place in the present of an external medium such as steam, air, oxygen or carbon dioxide and involves all chemical reactions between fuel, pyrolysis products and gasification medium. These reactions can be divided according to their phases into the heterogenous gas-solid or homogenous gas phase reactions. Gas-solid reactions include: the Boudouard reaction (1), the heterogenous water-gas reaction (2), the hydrogasification (3), the partial oxidation of carbon (4) and the oxidation of carbon (5). Homogenous gas reactions include water-gas-shift reaction (6), methanation reactions (7-9) and oxidation reactions (10-13). All above mentioned reactions with are listed below in Table 1.

Table 1: Main gasification reactions [8]

Heterogenous	Reaction
$C + CO_2 \leftrightarrow 2CO$	endotherm (1)
$C + H_2O \leftrightarrow CO + H_2$	endotherm (2)
$C + 2H_2 \leftrightarrow CH_4$	exotherm (3)
$C + 0.5O_2 \rightarrow CO$	exotherm (4)
$C + O_2 \rightarrow CO_2$	exotherm (5)

Homogenous		
$\text{CO} + \text{H}_2\text{O} \leftrightarrow \text{CO}_2 + \text{H}_2$	exotherm	(6)
$2\text{CO} + 2\text{H}_2 \leftrightarrow \text{CH}_4 + \text{CO}_2$	exotherm	(7)
$\text{CO} + 3\text{H}_2 \leftrightarrow \text{CH}_4 + \text{H}_2\text{O}$	exotherm	(8)
$\text{CH}_4 + 2\text{H}_2\text{O} \leftrightarrow \text{CO}_2 + 4\text{H}_2$	endotherm	(9)
$\text{CH}_4 + 0.5\text{O}_2 \rightarrow \text{CO} + 2\text{H}_2$	exotherm	(10)
$\text{CH}_4 + 2\text{O}_2 \leftrightarrow \text{CO}_2 + 2\text{H}_2\text{O}$	exotherm	(11)
$\text{H}_2 + 0.5\text{O}_2 \rightarrow \text{H}_2\text{O}$	exotherm	(12)
$\text{CO} + 0.5\text{O}_2 \rightarrow \text{CO}_2$	exotherm	(13)

Since only a small amount of oxygen is present in the reactor during gasification, the endothermic reactions are more dominant and hence heat is needed for the process. Depending on the energy input, gasification processes can be divided in autothermal and allothermal gasification. In autothermal gasification part of the fuel is oxidized within the gasifier and the released energy is used for endothermic gasification. In allothermal gasification the required heat for the process is produced outside the gasifier and carried in via e.g. circulating bed material, heat exchanger etc. Steam, air or carbon dioxide is commonly used as a gasification agent.

2.2.2.2. Dual Fluidized Bed Steam Gasification

Dual Fluidized Bed (DFB) Steam Gasification is an allothermal process with high energy efficiency developed at TU Vienna, Austria. The main advantage consists in the fact, that the product gas is free of nitrogen, what is achieved by dividing the reactor into two separate parts – the gasification reactor (GR) and the combustion reactor (CR). The principle of the DFB gasification system is shown in Figure 2.

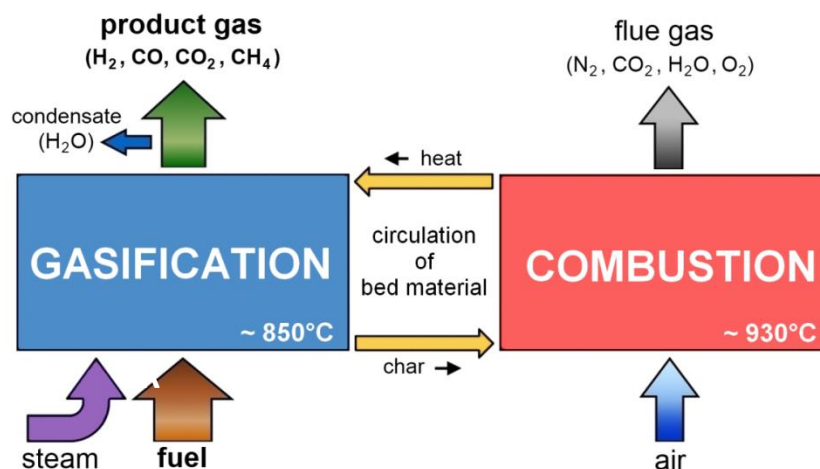


Figure 2: Principle of the DFB gasification system [9]

Bed material is fluidized in the gasification reactor with steam and the feedstock is gasified at approximately 850 °C. The required energy is supplied by a circulating bed material, which serves not only as an energy carrier but also as a catalyst. Bed material is then transported from the GR together with char (a solid product of gasification) via a chute into the combustion reaction (CR), where it is fluidized with air. Burning char provides energy for heating up the bed material, which is then transported back to GR, providing the heat necessary for the gasification reactions. After leaving the GR, the nitrogen-free product gas is further processed and cleaned downstream. Flue gas with a temperature of 930 °C from the CR can be used to heat up the steam (also for district heat) to increase the overall efficiency.

2.2.3. Combustion

Simplified, combustion is an exothermic redox reaction between a reductant (biomass) and an oxidant (air or oxygen). However, biomass combustion is a much more complex process, which includes several heterogeneous and homogeneous reactions and can be divided into 5 main steps: drying, devolatilization, gasification, char combustion and gas-phase oxidation. Typical power range of biomass furnaces varies from 2 kW (manual wood stoves or log wood boilers) to 100 MWe (circulating fluidized bed combustion). In the case of combined heat and power production (CHP), biomass is besides the heat converted also to the electricity typically in the Rankine steam cycle or in the Organic Rankine cycle (ORC) [10].

2.3. Ash chemistry

2.3.1. Ash transformation chemistry

Ash, an inorganic solid residue of thermochemical feedstock conversion, consists of many metal and non-metal elements, such as Si, Ca, Mg, K, Na, P, S, Cl, Al, Fe, Mn, N, Cu, Zn, Co, Mo, As, Ni, Cr, Pb, Cd, V and Hg. These are present in various amounts and have different importance in ash transformation reactions. In biomass, metals like Cu, Zn, Co, Mo, As, Ni, Cr, Pb, Cd, V and Hg comprise only a minority of the total amount of the ash and hence can be neglected in the considerations about ash transformation reactions in this chapter. Another simplification can be made with the exclusion of Fe and Mn from the considerations, since neither one of them plays

an important role in ash agglomeration. Thus, in the next chapter, only the effects of Si, Ca, Mg, K, Na, P, S, Cl and Al will be taken into the account.

According to Boström et.al [11], the ash related reactions can be divided into the primary, secondary and tertiary transformation reactions. The primary reactions refer to the reactions between ash-forming elements and oxygen. Based on the equilibrium data, several general descriptions can be made. The oxides of Ca, Mg and Si (CaO, MgO and SiO₂ accordingly) show high chemical stability at all operational temperatures and will stay in the solid state throughout the thermodynamic conversion of the fuel. However, at very high temperatures (caused by e.g. char burnout), SiO₂(s) can be reduced to SiO(g) and released into the flue gas. Phosphor is available in biomass in the form of various phosphates and can be released in the form of P₂O₅ (g) and possibly (if its introduced to reducing atmosphere) reduced to P₂O₃(g). Potassium and sodium are present in the biomass mostly in the form of salts. However, because of their low stability, they will be transformed to metal vapor at the elevated temperatures. Furthermore, they will react with water and form hydroxides KOH(g) and NaOH(g), which can (at CO₂ absence) partly condense as a liquid. Et elevated temperatures, sulphur is released either in the form of elemental sulphur S₂(g) or in the form of hydrogen sulfide H₂S(g) and subsequently oxidized to SO₂(g) or SO₃(g), depending on the oxygen surplus. From all ash-forming elements, only chlorine doesn't form stable oxides at operational temperatures, and is released from the biomass as Cl₂(g). Afterwards Cl₂(g) likely reacts with water, forming HCl(g).

Secondary ash transformations include already the mutual reactions between the ash-forming elements. The elements act either as Lewis base (electron donor) or Lewis acid (electron acceptor). The positively charged ions like K⁺, Na⁺, Ca²⁺, Mg²⁺, Al³⁺ and Fe^{2+/3+} act in reaction with a negatively charged oxygen ion O²⁻ (or OH⁻) as an electron acceptor (Lewis acid). The potassium ion K⁺ is due to its electronegativity the weakest Lewis acid among the above mentioned elements, and hence form the strongest Lewis base (as K₂O or KOH resp.) with the oxygen or hydroxide ion [12]. Both basic and acidic compounds are arranged in Table 2 by their relative strength. It is worth mentioning, that this order depends on the temperature and in some

situation can change. Moreover, this approach doesn't take into account the kinetic factors, fluidization conditions, aggregation, mass transport, etc.

Table 2: Relative Lewis acid/base potential [12]

Basic compounds	Acidic compounds
KOH(l,g) (K ₂ O)	P ₂ O ₅ (g)
NaOH(l,g) (Na ₂ O)	SO ₂ (g)/SO ₃ (g)
CaO(s)	SiO ₂ (s)
MgO(s)	HCl(g) (Cl ₂)
H ₂ O(g)	CO ₂ (g)
	H ₂ O(g)

However, this approach is useful as the first insight into the complex ash transformations. Thus, in most cases, the reactions will take place according to Table 2. For example, in the reaction, where P₂O₅ act as a base, K-phosphates will form prior to the Na, Ca, or Mg -phosphates. This rule is applicable also in the reversed scenario – if there is competition for the metal cations (for example K⁺) among the acids, initially potassium phosphates will form. Only after the P₂O₅(g) is consumed, the K- sulfates and K-silicates form.

In acidic compounds such as P₂O₅, SO₂/SO₃ and SiO₂, the central atoms P^{+V}, S^{+IV} and Si^{+IV} are strongly bonded to its own oxygen molecules. These acidic central ions are also able to form another bond with an additional oxygen entity, forming the negatively charged molecule, which is a crucial step in the secondary ash reactions. These ions then act as an electron donor in reaction with positively charged K⁺, Na⁺, Ca²⁺ ions. The main secondary ash-forming reactions are summarized in Table 3.

Table 3: Secondary ash reactions [11]

Secondary reactions	
P ₂ O ₅ (g) + 2KOH(g) ↔ 2KPO ₃ (l,g) + H ₂ O(g)	(14)
SO ₃ (g) + 2KOH(g) ↔ K ₂ SO ₄ (l,g) + H ₂ O(g)	(15)
SiO ₂ (s) + 2 KOH(g) ↔ K ₂ SiO ₃ (l,s) + H ₂ O(g)	(16)
HCl(g) + KOH(g) ↔ KCl(l,g) + H ₂ O(g)	(17)
P ₄ O ₁₀ (g) + 2 CaO(s) ↔ 2 CaP ₂ O ₆ (l,s)	(18)
SO ₃ (g) + CaO(s) ↔ CaSO ₄ (s,l)	(19)
SiO ₂ (s) + CaO(s) ↔ CaSiO ₃ (s,l)	(20)
2 HCl(g) + CaO(s) ↔ CaCl ₂ (s,l) + H ₂ O(g)	(21)

The negatively-charged ions (e.g. SiO_3^{2-} , PO_3^-) from the secondary reaction can react further in the tertiary reaction either as an acid or a base. A few examples of the tertiary ash reactions are shown below in Table 4.

Table 4: Tertiary ash reactions [12]

Tertiary reactions	
$2 \text{KPO}_3(\text{l},\text{g}) + \text{CaO}(\text{s}) \leftrightarrow \text{CaK}_2\text{P}_2\text{O}_7(\text{s},\text{l})$	(22)
$\text{CaK}_2\text{P}_2\text{O}_7(\text{s},\text{l}) + \text{CaO}(\text{s}) \leftrightarrow 2\text{CaKPO}_4(\text{s},\text{l})$	(23)
$2 \text{CaKPO}_4(\text{s},\text{l}) + \text{CaO}(\text{s}) + \text{H}_2\text{O}(\text{g}) \leftrightarrow \text{Ca}_3(\text{PO}_4)_2(\text{s},\text{l}) + 2 \text{KOH}(\text{g})$	(24)

2.3.2. Reactions of alkali metals with other species during thermochemical conversion processes

The relatively high concentration of potassium (compared to e.g. wood or coal) in the low ranking biomass ash is the main cause of the ash related problems such as agglomeration, slagging and corrosion. Potassium is present in the biomass in the form of salt or it can be bonded organically as a potassium ion. At elevated temperatures it is released into the gas phase either as a $\text{K}(\text{g})$, $\text{KOH}(\text{g})$ or $\text{KCl}(\text{g})$ and react readily with other gas species. If the chlorine is present in the gas, the most dominant potassium compound will be $\text{KCl}(\text{g})$. By the chlorine deficiency, $\text{K}(\text{g})$, $\text{K}_2\text{CO}_3(\text{g})$ or $\text{KOH}(\text{g})$ will be formed. $\text{KCl}(\text{g})$ can condense as KCl aerosol particle and with melting temperature of 770°C it can further melt at the furnaces surface. KCl also reduces the melting temperature of the fly ash. Alkali vapor species can undergo several possible gas-phase reactions, such as sulfation, chlorination and carbonation. The reactions are listed in Table 5.

Table 5: Gas-phase reactions of alkali species ("M" stands for either K or Na)

Sulfation reactions	
$2 \text{MOH}(\text{g}) + \text{SO}_2(\text{g}) + \frac{1}{2} \text{O}_2(\text{g}) \leftrightarrow \text{M}_2\text{SO}_4(\text{g}) + \text{H}_2\text{O}(\text{g})$	(25)
$2 \text{MCl}(\text{g}) + \text{SO}_2(\text{g}) + \frac{1}{2} \text{O}_2(\text{g}) + \text{H}_2\text{O}(\text{g}) \leftrightarrow \text{M}_2\text{SO}_4(\text{g}) + 2\text{HCl}(\text{g})$	(26)
$\text{M}_2\text{CO}_3(\text{g}) + \text{SO}_2(\text{g}) + \frac{1}{2} \text{O}_2(\text{g}) \leftrightarrow \text{M}_2\text{SO}_4(\text{g}) + \text{CO}_2(\text{g})$	(27)
Chlorination reactions	
$\text{MOH}(\text{g}) + \text{HCl}(\text{g}) \leftrightarrow \text{MCl}(\text{g}) + \text{H}_2\text{O}(\text{g})$	(28)
$\text{M}_2\text{CO}_3(\text{g}) + 2\text{HCl}(\text{g}) \leftrightarrow 2\text{MCl}(\text{g}) + \text{CO}_2(\text{g}) + \text{H}_2\text{O}(\text{g})$	(29)
Carbonation reactions	
$2\text{MOH}(\text{g}) + \text{CO}_2(\text{g}) \leftrightarrow \text{M}_2\text{CO}_3(\text{g}) + \text{H}_2\text{O}(\text{g})$	(30)

The products of these reactions can form in further reaction with silica the alkali silicates. Some of these reactions are listed below in Table 6.

Table 6: Silication reactions of alkali species

$M_2SO_4(g) + nSiO_2(s, l) \rightarrow M_2O \cdot nSiO_2(s, l) + SO_3(g)$	(31)
$M_2SO_4(g) + (2SiO_2 + Al_2O_3)(s, l)^* \rightarrow 2MAISiO_4(s, l) + SO_3(g)$	(32)
$2MCl(g) + (2SiO_2 + Al_2O_3)(s, l)^* + H_2O(g) \rightarrow 2MAISiO_4(s, l) + 2HCl(g)$	(33)
$2MOH(g) + nSiO_2(s, l) \rightarrow M_2O \cdot nSiO_2(s, l) + H_2O(g)$	(34)
$2MOH(g) + (2SiO_2 + Al_2O_3)(s, l)^* \rightarrow 2MAISiO_4(s, l) + H_2O(g)$	(35)

*oxides or compounds

2.4. Agglomeration

Agglomeration is a natural phenomenon caused by increased adhesion forces between particles, which force them to stick to one another and form agglomerates. In some cases it can be beneficial, for example in granulation process. However, in the case of FB gasification and combustion, it is a highly undesired process and can cause huge problems during the operation. In the worst case, if the agglomerates continue to grow uncontrollably, it can end with total defluidization of the bed.

Lower rank fuels, especially those from agricultural residues, contain high amounts of inorganics such as potassium, silica, calcium and sodium, which leads to higher contents of the ash within the reactor. The ash, as well as the ash-derived compounds (such as alkali silicates), can start to agglomerate already at operational process temperatures, depending on their melting temperatures and fluidization dynamics. In order to prevent the operational problems and unscheduled shutdowns, deeper and more extensive understanding of the ash transformation chemistry and the ash agglomeration mechanism is necessary.

2.4.1. Agglomeration mechanisms

Gatternig and Karl [13] summarized and divided agglomeration mechanisms as follows:

- a) Chemical reaction sintering
- b) Solid state sintering

- c) Melt induced agglomeration
- d) Coating induced agglomeration

In the first case (type a) agglomeration is caused by solid binding material, which is a product of gas-solid reaction. A typical representative in this case is carbonation of CaO.

The second type (b) can occur between particles of the same species, for example by iron (Fe). Agglomeration in this case is caused because of surface energy driven formation of necks between iron particles.

In the field of FB gasification and combustion the most dominant are type c) and d).

2.4.2. Melt-induced agglomeration

Melt-induced agglomeration takes place during the thermochemical conversion processes of biomass with a high amount of alkali metals such as potassium and sodium. At elevated temperatures, alkali may form alkali silicates in the reaction with SiO₂. With the melting temperature much lower than an optimal FB operation temperature (700-800 °C), these viscous melts create liquid bridges between the particles and held them together. Although melt induced agglomeration occurs in lesser extent than coating induced agglomeration, it is a serious issue in gasification and combustion, since the bed tends to defluidize much more rapidly. Moreover, during combustion this process is promoted also by increased temperature of the burning char, which can exceed bed temperatures by 200 °C, in some cases even by 600 °C [13].

2.4.3. Coating-induced agglomeration

The interactions between the bed material particles and ash from biomass leads to the covering of bed material with a thin layer composed of alkali and silica (depending on the ash and the bed material), which at elevated temperatures melts and cause sticking of particles together upon collision. This process is called coating induced agglomeration and is the most common agglomeration in the field of FB combustion and gasification. Ash and the bed material can create an eutectic system

with low melting temperature (in some K-silicate system already at 600 °C) which also promotes sintering at elevated temperatures in the fluidized bed [3].

The melt and coating induced agglomeration mechanisms are displayed below in Figure 3.

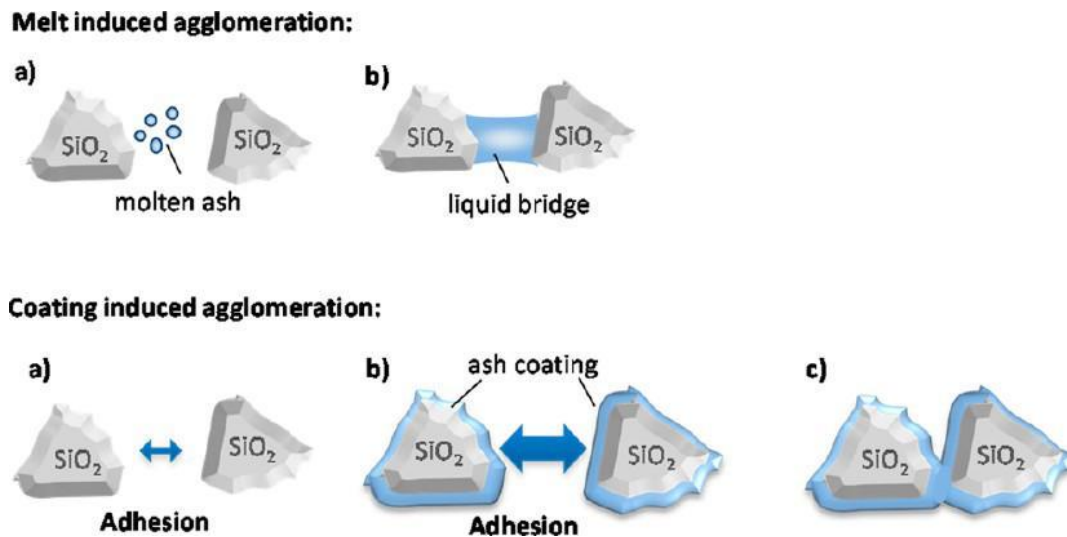


Figure 3: Melt- and coating induced agglomeration mechanism [13]

2.5. Layer formation

The formation of layer differs between various bed materials. These layers play a crucial role in the agglomeration process. Currently most used bed materials are quartz sand, feldspar and olivine. Since it appears, that the layer formation on feldspar and olivine are based on similar mechanism [14], only olivine from those two will be described in the next chapters.

2.5.1. Quartz

As mentioned before, the interactions between ash and bed material leads to the formation of a thin layer on the particle surface. The formation of this layer starts with attachment of ash onto the quartz surface (Figure 4). This could be performed by either direct collision of the molten ash from the burning char with the bed material, or by condensation of gaseous alkali on the particle surface. Afterwards the attached

ash together with silica from quartz sand form a low melting alkali silicate – a sticky layer, that at some critical thickness bonds particles together and cause agglomeration of the bed [15].

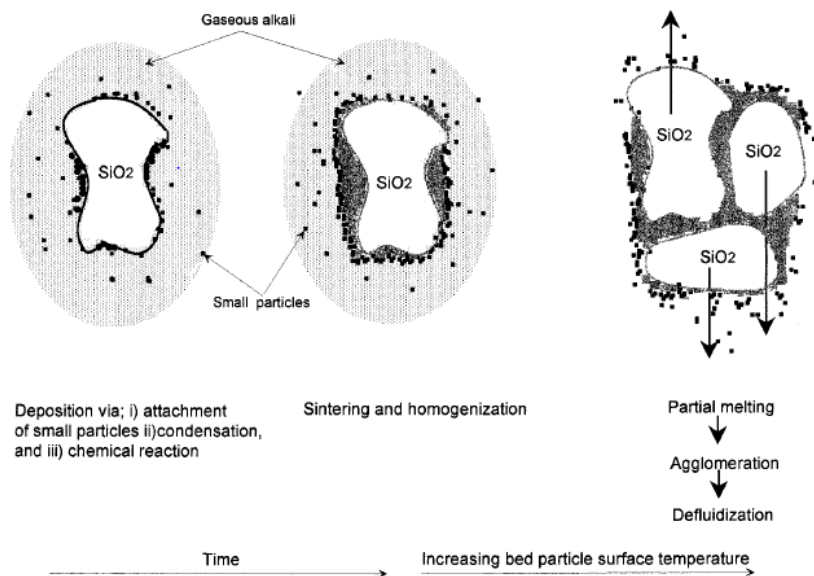


Figure 4: Sub-processes of the bed agglomeration mechanism [16]

It has been observed, that particles are not surrounded just by one, but by multiple layers with different elementary compositions. Whereas outer layers are relatively inhomogeneous and their composition is very similar to fuel ash, the inner layer can be considered homogenous, and its composition depends on both, fuel and bed material.

According to He et al. [15], formation of layers starts with reaction of alkali with the bed particle surface. This reaction leads to a formation of outer potassium-silicate layer with low melting temperature. Calcium, which is present in flying ash, is then attached on this molten outer layer and diffuses through the K-silicate layer. Under the outer layer (i.e. on the particle surface) it reacts with quartz, forming an inner layer of Ca-silicates. Upon further calcium delivery from the ash also more complex calcium silicates like Ca_2SiO_4 or Ca_3SiO_5 will be formed. The inner layer will continue to grow towards the bed material core, until diffusion is the limiting step. That results in the shrinking of the unreacted quartz particle core.

Besides agglomeration, other major problem caused by layer build-up on the quartz sand is the formation of cracks in the particles. He et al. [17] studied this matter in

more detail, proposed a mechanism for the crack layer formation. The whole process happens in 3 phases. Phase 1 includes the formation of a thin layer on the particle surface, as described above. During phase 2, thanks to microstructural stress caused by calcium silicates, cracks inside this layer will appear and spread inwards the particle core due to the tension forces. These cracks allow gaseous potassium to diffuse inside the particle and react with silica, possibly forming K-silicate melts. In phase 3, as the cracks grow wider, some of the inner layer will break off and expose the particle surface. This allows the gaseous potassium to react with the silica even further, enhancing the growth and the connection of the cracks. The process ends up with the break-down of the whole particle, what causes undesirable and problematic deposit build-up in cyclones and cyclone legs. To avoid clogging, bed material needs to be regularly replaced, what results in the increase of the overall operation costs. The scheme of crack formation is shown in Figure 5.

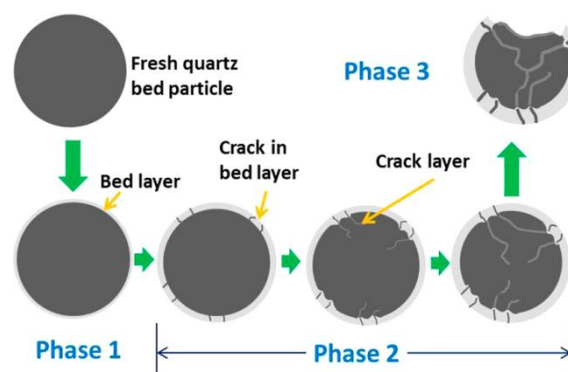


Figure 5: Mechanism of the crack formation [17]

2.5.2. Olivine

Because of his catalytic activity and also high resistance to attrition (compared to, for example, limestone), olivine has been used as a bed material in several industrial gasification plants. It has been observed, that two layers were formed on the bed material surface, composed mainly of calcium.

Kuba et al. [18] proposed a mechanism of the layer formation on olivine, which differs significantly to the one for quartz sand. Olivine is a material with two main

components, fayalite (Fe_2SiO_4) and forsterite (Mg_2SiO_4), and with an orthorhombic structure. This structure has two octahedral metal sites, both occupied by either an iron (Fe^{2+}) or a magnesium (Mg^{2+}) ion. In the proposed mechanism these sites are attacked and replaced by calcium ion (Ca^{2+}) from biomass ash. Such exchange of metal ions is enabled above temperatures of $600\text{ }^\circ\text{C}$ [18]. Since substitution of Fe^{2+} with Ca^{2+} is more likely than that of Mg^{2+} , it will be diluted from the crystal structure first. With additional feed of calcium, Ca^{2+} starts to substitute Mg^{2+} and release it from the octahedral site. However, unlike the Fe^{2+} , Mg^{2+} is trapped and accumulated between inner and emergent outer calcium layer. This leads to the formation of Mg-rich crack zones (Figure 6).

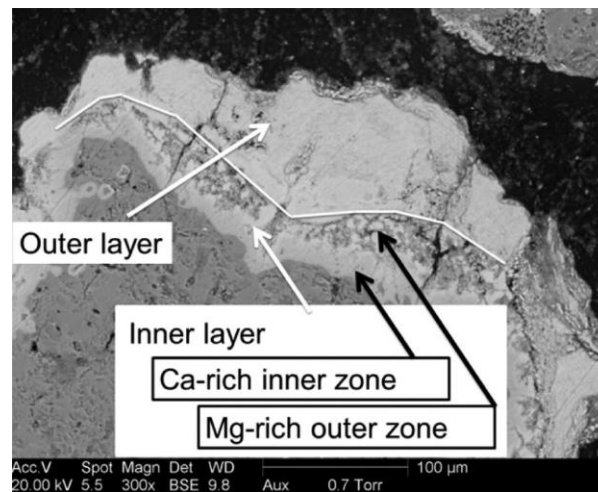


Figure 6: ESEM image with inner and outer layer on olivine bed particle [18]

Moreover, the results of this study also show that potassium doesn't form layers on the olivine surface, which has been also confirmed by thermochemical equilibrium calculations. However, potassium still tends to react with silica from the ash, forming low melting temperature silicates, which can cause the melting-induced agglomeration.

Although olivine shows good catalytic activity and resistance to agglomeration, his long term application as a bed material is undesirable, since it contains heavy metals like nickel and chromium, which, due to the attrition, ends up in ash. Subsequent disposal of ash, that is rich in these heavy metals, is difficult and considerably increases operation costs.

2.6. Methods of agglomeration determination

Several methods are used to determine the agglomeration temperature in fluidized bed. Skrifvars et al [19] compared three often used experimental techniques for agglomeration determination – an ash fusion test (ASTM), a compression-strength - based sintering test and the controlled fluidization bed agglomeration method.

2.6.1. The ASTM ash fusion test method

The ASTM ash fusion test is a standardized method based on the visual indication of the softening and melting behavior of a test sample. During the test, an ash pellet is heated in an electric furnace and 4 characteristic temperatures are visually determined – the initial deformation temperature, the softening temperature, the hemispherical temperature and the flow temperature (Figure 7). The start of the agglomeration is assigned to the initial deformation temperature [19].

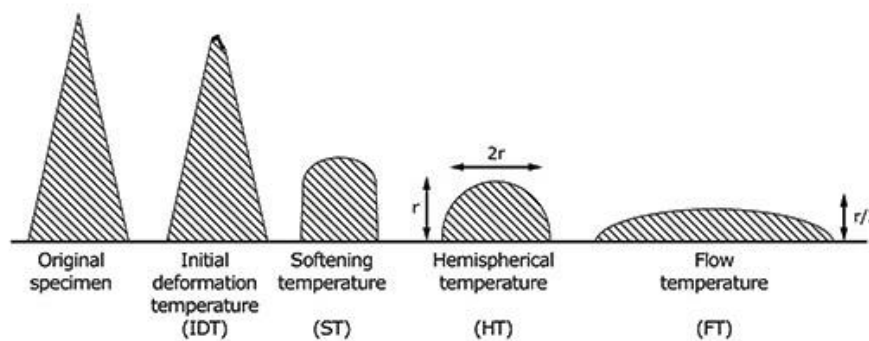


Figure 7: Characteristic shapes of a test particle

2.6.2. The Sintering Test Method

During the sintering test, the pellet is heated up in an electric tubular furnace to a certain temperature and afterwards its strength is determined by a standard compression strength testing device. This test can be carried out directly after heating at high temperatures, or at room temperature after the pellet is cooled down. However, in the latter case, an additional set of tests (i.e. zero tests) needs to be performed, in order to determine temperature-strength dependency [19]. The

sintering temperature T_{sint} is defined from a compression-strength vs. temperature curve as the temperature range, where the pellets strength is increased due to increased inter-particle material bonds and due to filling of the void fraction.

2.6.3. The Controlled Fluidized Bed Agglomeration Method

The Controlled Fluidized Bed Agglomeration Method was developed by Öhman and Nordin [20]. The test was carried out with a bench scale fluidized bed reactor with the electrical power of 5 kW. The reactor is 2 m high and the diameter spreads from 100 mm (bed) to 200 mm (freeboard). At the beginning of the experiment, the fuel is fluidized and burned with air, till sufficient ash amount is produced (approx. 6%). This phase is called “ashing”. Afterwards the fuel feeding is stopped and the temperature is linearly increased through external heating (mixture of propane and air is used in the combustion chamber and led through the air distributor into the reactor). The initial agglomeration temperature T_{agg} is determined by a sudden temperature and pressure drop in the bed. The schematic of the bench scale FB is shown in Figure 8.

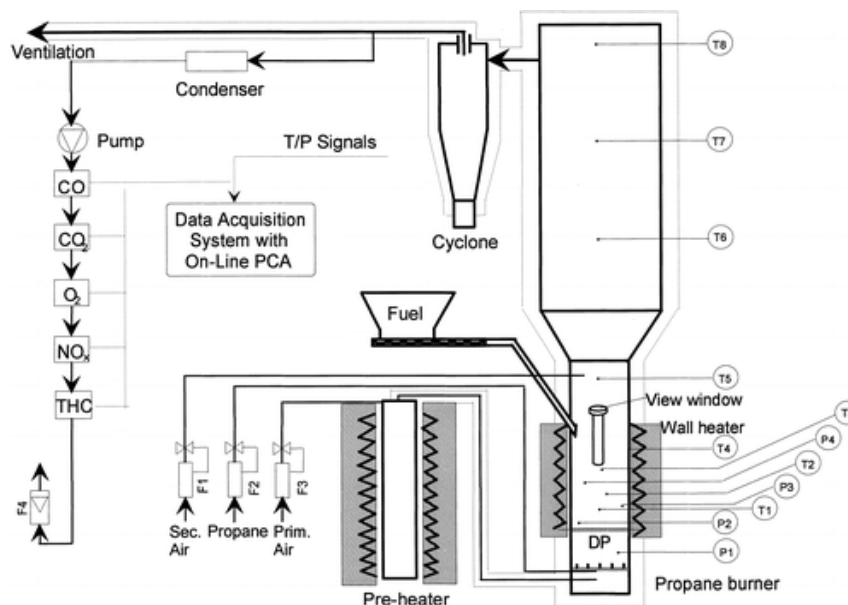


Figure 8: Schematic of the bench scale FB reactor [20]

2.6.4. Comparison of the methods

In their research work [19], Skrifvars et al. compare mentioned techniques to determine the agglomeration temperature of 10 different fuels: wheat straw, olive

flesh, peat, bagasse sugar cane, cane trash, forest residue (soft wood), reed canary grass, Lucerne grass, bark and RDF community waste. The results are summarized in Table 7.

Table 7: Comparison of the methods by Skrifvars et al. [19]

	Unit	IDT	ST	HT	FT	T _{sint}	T _{aggl}
wheat straw	[°C]	900	1040	1170	1190	680–700	740
olive flesh	[°C]	1100	1170	1190	1200	800–900	930
peat	[°C]	1100	1160	1180	1200	1000–1100	>1020
bagasse	[°C]	1260	1380	1430	1480	850–900	>1020
cane trash	[°C]	1150	1200	1350	1480	850–950	996
forest residue	[°C]	1150	1200	1210	1220	>1000	982
reed canary grass	[°C]	1260	1520	1560	>1600	680–700	920–970
Lucerne	[°C]	1550	1580	>1600	>1600	625–650	670
Bark	[°C]	1340	1540	1540	1540	>1100	988
RDF	[°C]	1090	1190	1220	1240	800–900	990

In all ten cases, the ASTM fusion test fails to predict the agglomeration behavior of the examined ash in FBC, since it shows the agglomeration temperatures much higher than typical FBC operational temperatures (800-900 °C). This is caused by the absence of the interactions between the particles. The sintering test provides more accurate results, since it include also the interactions between the ash particles in solid and gaseous phases. More accurate predictions can be achieved by The Controlled Bed Agglomeration Method (2.6.3). However, as Scala [21] remarked, the effect of the local overheating due to the burning char particles and the progressive accumulation of the ash in bed is absent in this method, which can cause deviations from the full scale FBC units.

3. Materials and Methods

3.1. Fuel and bed material preparation

3.1.1. Fuel preparation

Wheat straw and wheat straw lignin have been used as feedstock. To produce wheat straw and lignin pellets, the pelletizer PP200 from company Cissonius with an electrical power of 7.5 kW was used (Figure 9). Quality of the pellets, which can be described by their strength and durability, is strongly affected by the fuel constituents. Components like starch, protein and lignin act as a natural binder and have a positive effect on the pellet properties. On the other side, resilience characteristics (elasticity and stiffness) of the water-insoluble fibers cause pellet fragmentation and hence decrease pellets quality. Usually, feed is preheated either directly (through steam conditioning), or indirectly (through electrical heater), since elevated temperatures activate binders and lubricants in the fuel and also promote gelatinization of starch and denaturation of protein [22].



Figure 9: Pelletizer from company Cissonius with electrical power of 7.5kW

Due to the fact, that lignin is a natural binder, no problem emerged during its pelletizing. However, in the case of wheat straw, the pellets needed to be passed through the pelletizer's matrix several times, which considerably increased the pelletizing time. Another issue that occurred during the process was choking of the matrix. Both problems were caused by the composition of the feedstock- since straw is rich on hydrophobic waxes and has low lignin content, higher pelletizing

temperatures are required (50-100 °C) [23]. Without feed preheating or steam conditioning, this temperature needs to be achieved by mechanical attrition inside the matrix and hence, in order for fuel to be enough heated, pelletizing in multiple steps was necessary. Afterwards the pellets have been dried with air and stored. Figure 10 shows lignin before and after the pelletizing.



Figure 10: Wheat straw lignin before and after pelletizing

3.1.2. Fuel analysis

Table 8 shows some important parameters of both fuels, obtained by corresponding standard methods (water content by DIN 51718; ash content by EN ISO 18022; volatiles by EN ISO 18023; lower heating value by DIN 51900 T2; initial deformation temperature by CEN/TS 15370-1).

Table 8: Important parameters of wheat straw and lignin (d.b.-dry basis)

Parameter	Unit	Wheat straw	Lignin
		Value	
Water content	[wt.%]	7.2	6.06/24.39*
Ash content (d.b.)	[wt.%]	7.5	15.47
Volatiles (d.b.)	[wt.%]	74.7	64.88
Lower heating value LHV (d.b.)	[kJ/kg]	16860	18779
Initial deformation temperature	[°C]	830	755

*6.06 wt.% corresponds to the pelletized fuel; 24.39 wt.% to the non-pelletized

Furthermore, a XRF analysis of the fuel ashes was performed by Test Laboratory for Combustion Systems at TU Vienna with the Axios Advanced Analyser from company Panalytical. The mass of individual elements were measured and afterwards recalculated to oxides (Table 9).

Table 9: XRF analysis of wheat straw and lignin ash

Oxid	Unit	Wheat straw	Lignin
ZrO ₂	[wt.%]	0.03	0.02
SrO	[wt.%]	0.09	0.07
PbO	[wt.%]	n.n.	n.n.
As ₂ O ₃	[wt.%]	n.n.	n.n.
ZnO	[wt.%]	0.04	0.04
CuO	[wt.%]	0.14	0.04
NiO	[wt.%]	0.05	0.02
Co ₃ O ₄	[wt.%]	n.n.	n.n.
Fe ₂ O ₃	[wt.%]	1.81	0.71
MnO	[wt.%]	0.06	0.07
Cr ₂ O ₃	[wt.%]	0.04	0.08
V ₂ O ₅	[wt.%]	n.n.	n.n.
TiO ₂	[wt.%]	0.12	0.10
CaO	[wt.%]	4.43	3.76
K ₂ O	[wt.%]	12.26	3.08
Cl	[wt.%]	3.59	0.58
SO ₃	[wt.%]	5.30	1.27
P ₂ O ₅	[wt.%]	2.71	1.23
SiO ₂	[wt.%]	60.88	84.46
Al ₂ O ₃	[wt.%]	1.52	2.62
MgO	[wt.%]	4.32	0.35
Na ₂ O	[wt.%]	2.56	1.48

Table 10 shows results from an elemental analysis, performed at Microanalytical Laboratory at Institute for Physical Chemistry at TU Vienna with the 2400 CHN Elemental Analyzer from company Perkin Elmer. Additionally, total sulfur and chlorine content was determined by the standard method EN ISO 16994.

Table 10: Elemental analysis of wheat straw and lignin

Element (d.b.)	Unit	Wheat straw	Lignin
		Value	

Carbon	[wt.%]	45.09	51.67
Hydrogen	[wt.%]	5.75	3.49
Nitrogen	[wt.%]	0.55	1.43
Sulfur	[wt.%]	0.12	0.123
Chlorine	[wt.%]	0.09	0.025
Oxygen	[wt.%]	48.4	43.26

3.1.3. Bed material preparation

As bed material, quartz with mean diameter d_p of 450 μm [24] from the company Quarzwerke has been used. In order to achieve the desired range of the particles' diameter quartz sand was sieved on a vibration sieve from company Fuchs Mühlen (Figure 11) prior to the experiments.



Figure 11: Vibration sieve from Fuchs Mühlen

3.2. Descriptions of the fluidized bed reactors

Investigations of ash behavior in fluidized bed in oxidizing atmosphere (combustion) have been performed in the lab-scale and the bench-scale reactor. Behavior of wheat straw lignin ash during steady state operation in reducing atmosphere (gasification) has been further investigated in 100kW DFB pilot-plant.

3.2.1. Lab-scale fluidized bed reactor

Schematic of the lab-scale fluidized bed (FB) reactor is shown in

Figure 12.

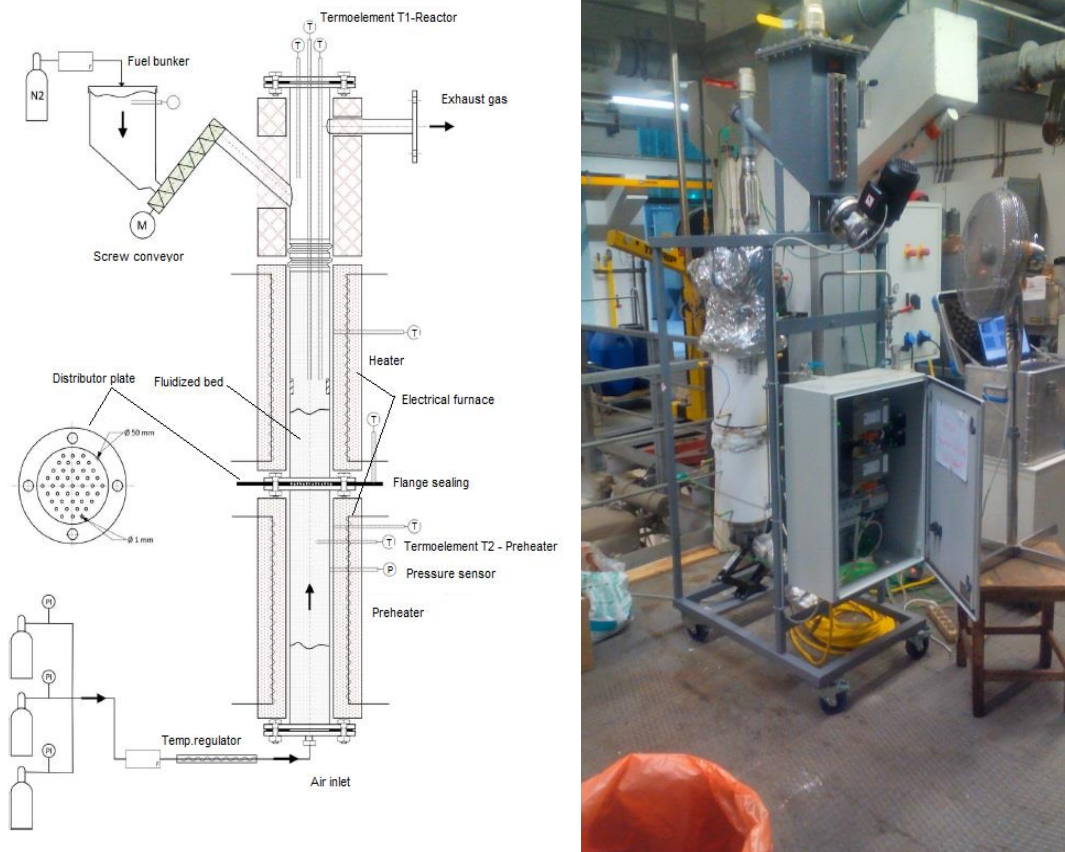


Figure 12: Lab-scale FB reactor, schematic drawing and photograph [24]

The lab-scale FB reactor with an inner diameter of 5.31 cm and a bed height of 10 cm is made of stainless steel. Before air is distributed into the reactor through a perforated plate, it is heated with a Microprocessor Temperature Regulator from the company Horst and with cylindrical electrical furnace with the power of 750W (preheater). The fluidizing section is heated up with a uniform cylindrical electrical furnace (reactor heater). Air volume flow can be regulated through a ball valve from 6.2 NI/min to the maximum of 40 NI/min. The reactor is sealed from the bottom with the KLINGERmilam PSS flange sealing with a maximum temperature of 900 °C. Five K-type thermocouples monitorise the temperatures of the fluidized bed, freeboard, fuel bunker, flange sealing as well as the temperature of preheaters and reactors wall. However, the reactor heater and preheater temperatures are not recorded and serve only as an input for PID temperature controllers. Air pressure is measured with

a pressure sensor situated between the air preheater and the distribution plate. Since the pressure in the freeboard section is defined by the chimney (below 1 bar), the change in the measured pressure corresponds also to the pressure change in the bed. Fuel pellets are transported from the fuel bunker into the reactor with a screw conveyor with AEG electromotor (0.18 kW) with the minimum rotation of 0.1rpm, which corresponds to the fuel input of approx. 300 g/h (depending on the fuel). Minimal fluidization velocities U_{mf} as well as the corresponding volume flows V_{mf} at 20 °C and 850 °C are shown in Table 11.

Table 11: Minimal fluidization velocity and corresponding air volume flow at 20 and 850 °C

Parameter	Unit	Value
U_{mf} (20 °C)	m/s	0.08
V_{mf} (20 °C)	l/min	10.4
U_{mf} (850 °C)	m/s	0.03
V_{mf} (850 °C)	l/min	1.1

3.2.2. Bench-scale reactor

The bench-scale fluidized bed reactor with its schematic is shown in Figure 13.

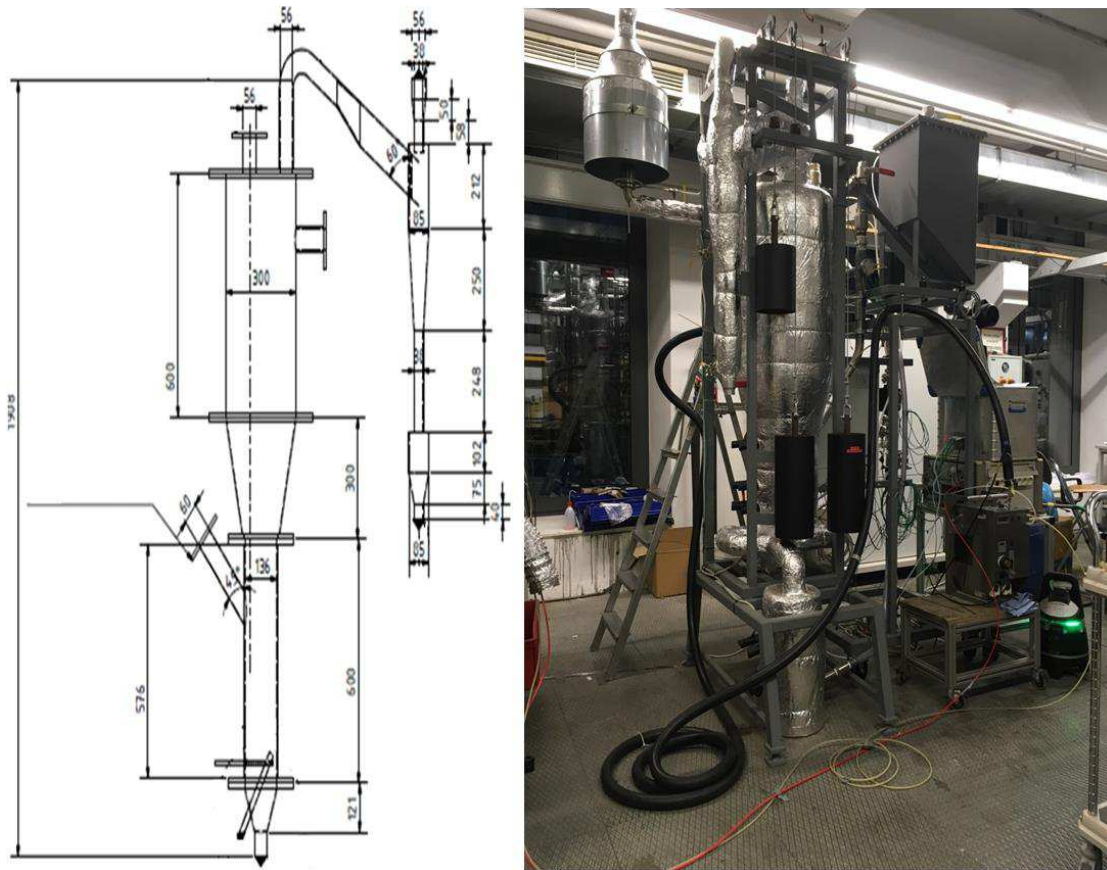


Figure 13: Bench-scale reactor, schematic drawing and photograph

The cylindrical FB reactor is made of stainless steel with an inner diameter of the fluidized bed section of 13.6 cm and the freeboard section with a diameter of 30 cm. The feedstock can be supplied continuously by two separate screw conveyors from 2 individual bunkers, with the volumes 15 l and 100 l. Both bunkers are flushed with N_2 in order to secure an inert atmosphere in the bunker and screw conveyor. The distribution of the air is realized through the air nozzles at the bottom of the reactor. For air preheating, a cylindrical air-preheater with the power of 1300 W is used. The pre-heater is able to increase the air temperature up to the 1150 °C. The air flow between 100-400 NI/min secures the bubbling bed regime and total combustion of the fuel. Produced gas is led from the reactor to the cyclone, where the ash is separated from the gas stream. Part of the gas is also bypassed to the 5-component gas analyzer, where the content of the O_2 , CO_2 , CO , H_2 and CH_4 is continuously measured. The remaining part of the gas is fed to the torch, where it is being burned with a CH_4 flame. Minimal fluidization velocities U_{mf} as well as the corresponding volume flows V_{mf} at 20 °C and 850 °C are shown in Table 12.

Table 12: Minimal fluidization velocity and corresponding air volume flow at 20 and 850 °C

Parameter	Unit	Value
U_{mf} (20 °C)	m/s	0.1
V_{mf} (20 °C)	Nl/min	197
U_{mf} (850 °C)	m/s	0.015
V_{mf} (850 °C)	Nl/min	27.6

3.2.3. 100kW DFB pilot-plant

The principle of the DFB gasification system has already been described in Chapter 2.2.2.2. 100kW DFB pilot-plant consists of two separate reactors: a gasification reactor (GR) and a combustion reactor (CR). The reactors dimensions are shown in Figure 14. Feedstock is introduced from the bunkers into the lower gasification reactor through a screw feeder, where it is fluidized with steam (bubbling bed regime). The product gas is then transported through the upper gasification reactor into the gravity separator, where the gas is separated from the bed material. The GR is connected with the CR via the upper loop seal and the lower loop seal. The bed material in the CR is fluidized with air (fast fluidization). The heat, necessary for the gasification reactions, is produced by combustion in the CR and transported into the GR via bed material. The fine ash is removed from both cyclones regularly, the coarse ash from the lower loop seal at the end of the experiment. Product gas and flue gas composition is continuously measured by an online gas measurement equipment Rosemount NGA200. The compounds ethane, ethane, propane are furthermore measured by a gas chromatograph from Perkin Elmer in 15 min intervals. Tars are isokinetically sampled (discontinuously) and afterwards measured by the gas chromatography mass spectrometry (GCMS).

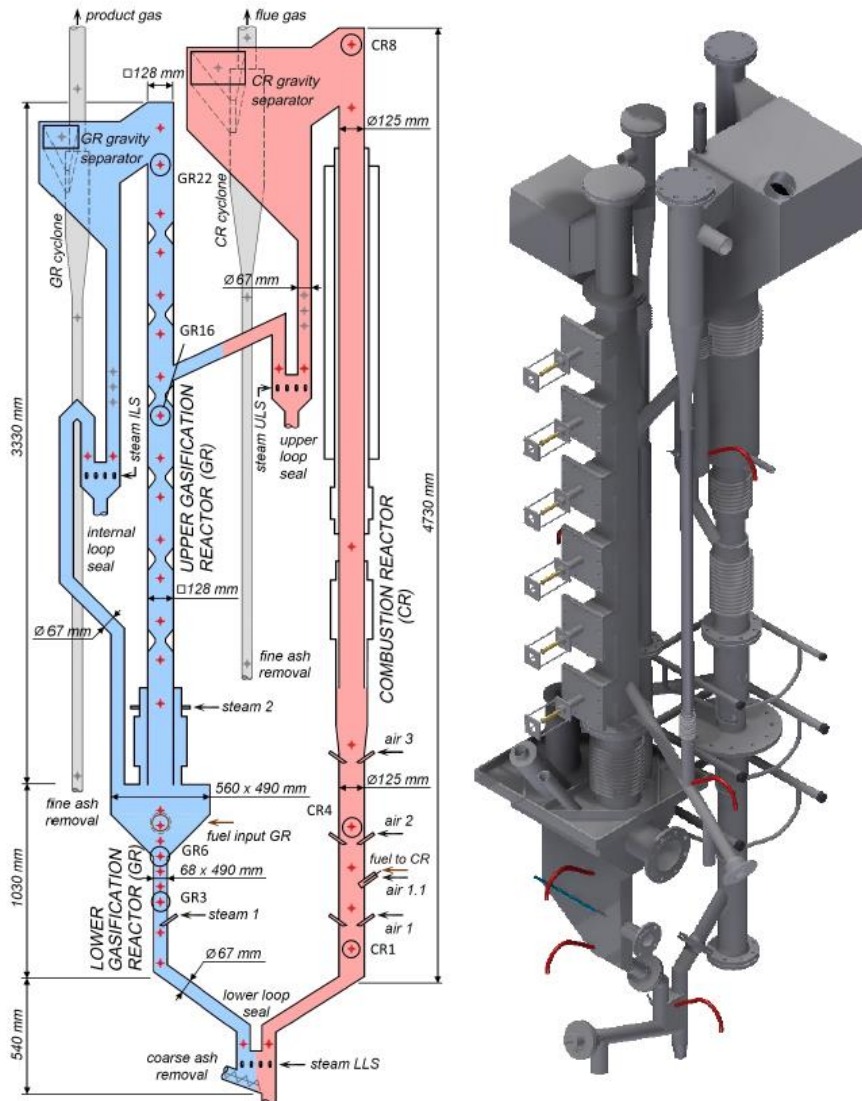


Figure 14: Novel 100 kW DFB pilot-plant

3.3. Developed method for determination of ash behavior in FB conversion processes

The new developed method for determination of ash behavior in the FB reactors is described in the next chapters. Unlike the method proposed by Öhman and Nordin this one also take into account the influence of the local overheating caused by burning char particles and of progressive accumulation of ash in the bed.

3.3.1. Experiments in the lab-scale reactor

The method used in experiments in the both, lab-scale and bench-scale reactor, consists of two separate parts. In the first part the ash is produced in the reactor through the fuel combustion. For both experiments wheat straw and wheat straw lignin have been used as a fuel. Approx. 300 g/h of the pellets have been supplied into the reactor by the screw conveyor. 300 grams of quartz with a mean particle diameter of 450 μm has been used as a bed material. The bed material has been fluidized with 20 NI/min of air. The bed temperature has been held between 600-650 $^{\circ}\text{C}$. After approx. 1 hour, the external heater is turned on and the temperature of the bed is increased in steps of 50 $^{\circ}\text{C}$ (part 2) until reaching the bed temperature of 950 $^{\circ}\text{C}$. Hence, the main difference between this method and the method proposed by Öhman and Nordin is the inclusion of the fuel combustion in the second phase of the experiment. Subsequently the burning char promotes the melting of the inorganics within the ash due to local overheating [15]. The absence of combustion in the second part, where the bed temperature is increasing, can lead to the inaccuracy in the agglomeration behavior of the fuel between lab-scale and full scale FBC unit [23].

3.3.2. Experiments in the bench-scale reactor

The same method as described in the chapter 3.3.1 has been used for the experiments in the bench-scale reactor. However, in the case of lignin, the experiment consisted only of the ashing phase at approx. 700 $^{\circ}\text{C}$. The experiment with the wheat straw included also the phase with the bed temperature increase.

The first set of experiments in the bench-scale reactor was conducted with lignin (both pelletized and non-pelletized material), the second one with the pelletized wheat straw. In both cases, 5500 grams of quartz have been used as a bed material. 200 NI/min of air has been used as a fluidizing medium, insuring the bubbling bed regime in the reactor. In the case of non-pelletized lignin and wheat straw, the fuel input of approx. 13 g/min has been supplied continuously at 30-40 Hz (depending on the fuel). As for the pelletized lignin, on-off- operation was necessary, since the heat produced during the combustion rapidly increased the bed temperature. The temperatures and the pressure in the reactor have been continuously measured, as well as the product gas composition.

3.4. Behavior of lignin ash in a steady-state operation in 100kW DFB pilot-plant

In order to investigate behavior of wheat straw lignin ash in a steady state operation in reducing atmosphere an experiment in 100kW DFB pilot-plant reactor has been performed. At the beginning of the experiment, both reactors were heated with the electrical heaters, followed by combustion of heating oil and softwood pellets. During the heating phase, air was used as fluidizing medium in both reactors. Afterwards the fluidization medium in GR was gradually switched from air to steam. In case of lignin, a gasification steam to fuel ratio of $1.0 \text{ kg}_{\text{steam}}/\text{kg}_{\text{fuel,db}}$ and a feedstock mass flow of 19.7 kg/h was used [25]. Prior to the lignin gasification, softwood has been used as a benchmark feedstock. The temperature and the pressure were continuously measured at different points of the GR and the CR. The compositions of the product gas and the flue gas were measured continuously; tar content was measured during the stable operation points. Both cyclones were regularly emptied and ash samples were collected. Additionally, a sample from the lower loop seal was taken at the end of the experiment.

3.5. Equilibrium calculations in Factsage

Additionally to experiments in the reactors described above, thermo-chemical equilibrium calculations were performed using the software Factsage 7.2. Factsage 7.2 is a fully integrated thermochemical software and database package, originally designed for simulations in pyrometallurgical industry. However, through its universality, it has also found to be suitable in combustion, geology, hydrometallurgy, corrosion, glass technology, ceramics etc. [26].

Calculations are carried out in the Equilib module, which employs the Gibbs energy minimization algorithm and thermochemical functions. The computation requires three entries:

1. Definitions of reactants
2. Selection of possible compounds and solutions on the product side
3. Setting of the final conditions (e.g. temperature and pressure)

As the reactants, the ash composition of the fuels ash has been used (Table 9). The amount of oxygen, necessary for total combustion, has been subsequently calculated in Factsage. FactPS, FToxid and FTsalt have been chosen as databases. FactPS contains data for 4869 compounds (pure substances). FToxid is a database for all pure oxides solutions of SiO_2 , Al_2O_3 , CaO , MgO , FeO and Fe_2O_3 , including some of their combination with oxides like, Cu_2O , K_2O , Na_2O , MnO , Mn_2O_3 , P_2O_5 , ZnO etc. FToxid-SLAGA has been chosen as the liquid (glass) solution and contains 2 separate solutions – SLAGA#1 and SLAGA#2. Final amount of calculated slag solution is combination of SLAGA#1 and SLAGA#2. Finally, FTsalt contains data for the pure salts, as well as the salt solutions formed among ions like Na, K, Mg, Ca, NH_4 , Mn, Al, Fe(II), Fe(III), F, Cl, I, NO_3 , OH, SO_4 , CO_3 etc. The liquid (molten) phase is called FTsalt.

The pressure of 1 bar and temperature range between 650-1000 °C has been used as the initial conditions for both fuels.

4. Results

4.1. Lab-scale FB reactor

4.1.1. Wheat straw

With the method described in Chapter 3.3 experiments for both fuels - wheat straw and lignin were performed. Both experiments were conducted with 300 g of the bed material (quartz) and the fuel supply of approx. 300 g/h.

The results of the experiment with wheat straw are shown below in Figure 15 and Figure 16. As can be seen at both diagrams, the bed collapses (defluidize) at approx. 03:30. This time corresponds to the bed temperature of 865 °C and an ash content of 20 wt.%_{db}. After the reactor was cooled down and opened, agglomerates were found in the bed (Figure 17).

Prior to the experiment described above, an (unsuccessful) experiment with 50 grams of bed material was performed. Although the experiments also ended up with a bed agglomeration, the results are not applicable due to the fact, that the thermocouples did not detect the start of the agglomeration and the bed temperature were further increased till 950 °C. The theoretical ash content at this point equates to approx. 50 wt.%_{db}. At the end of the experiment, single large agglomerate was found glued to the reactor walls (Figure 18).

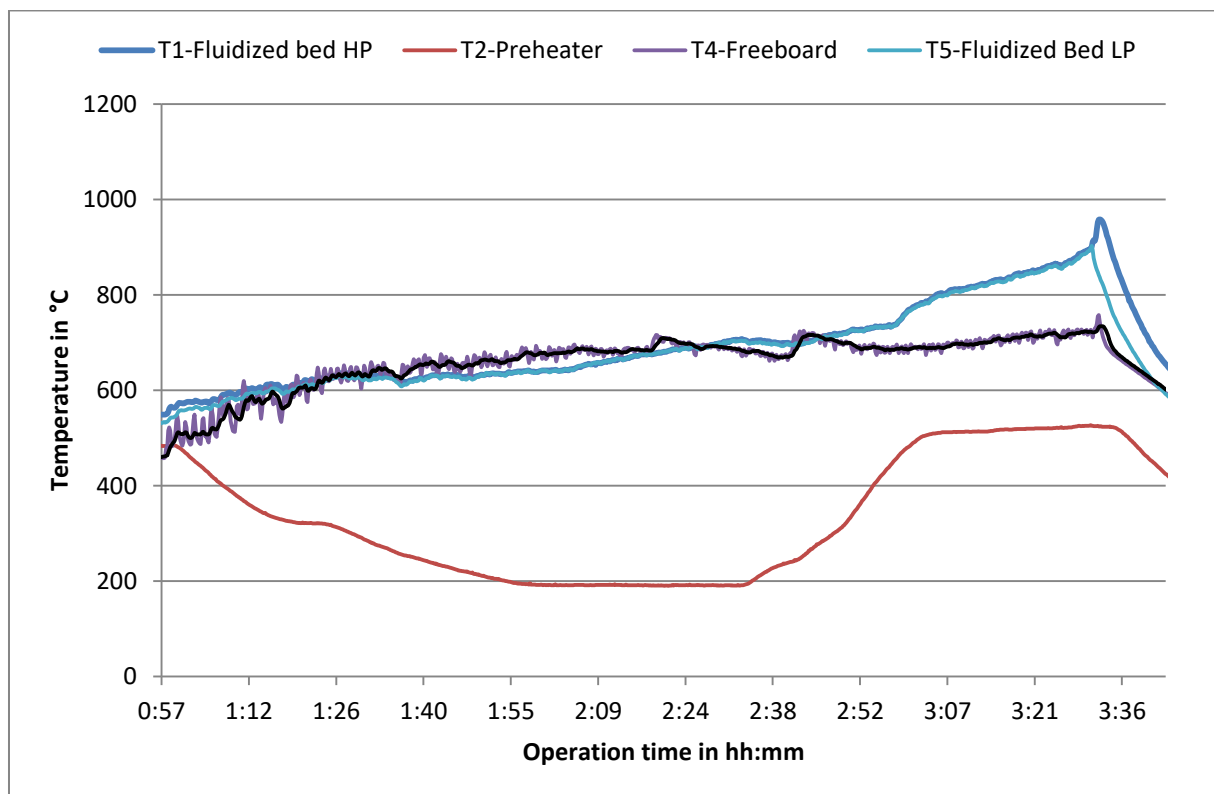


Figure 15: Temperature profile of wheat straw combustion in the lab-scale reactor

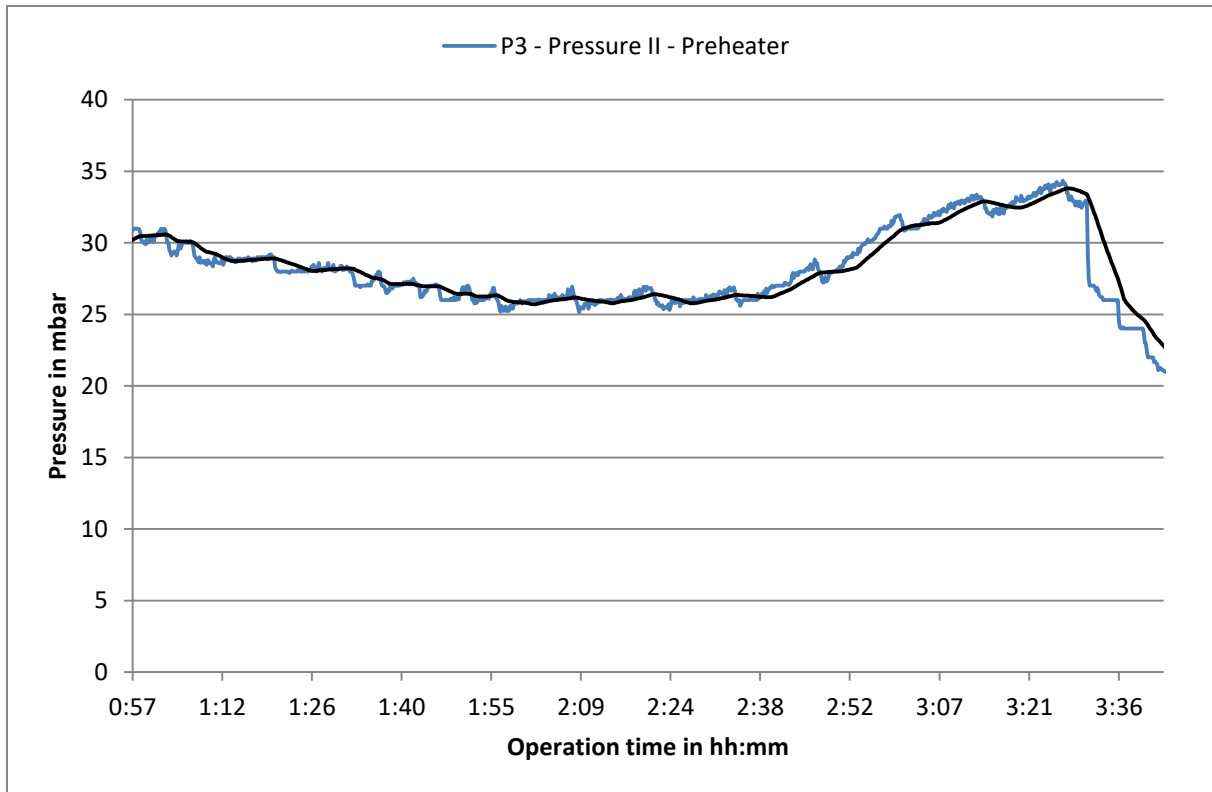


Figure 16: Pressure profile of wheat straw combustion in the lab-scale reactor



Figure 17: Wheat straw combustion - the agglomerates (left) and the bed material (right); 300 g of bed material



Figure 18: Wheat straw combustion - single large agglomerate; 50 g of bed material

4.1.2. Lignin

The experiment with lignin started with the ashing for approx. 1 hour. The amount of ash in the reactor after 1 hour corresponds to approx. 7% (with no regards on the ash that has been carried out from the reactor). The temperature of the bed has been afterwards continuously increased with an electrical heater (Figure 19). At approx. 4:22 (overall operating time, including the initial heating of the reactor) pressure fluctuations occurred (Figure 20) and the fuel supply was turned off.

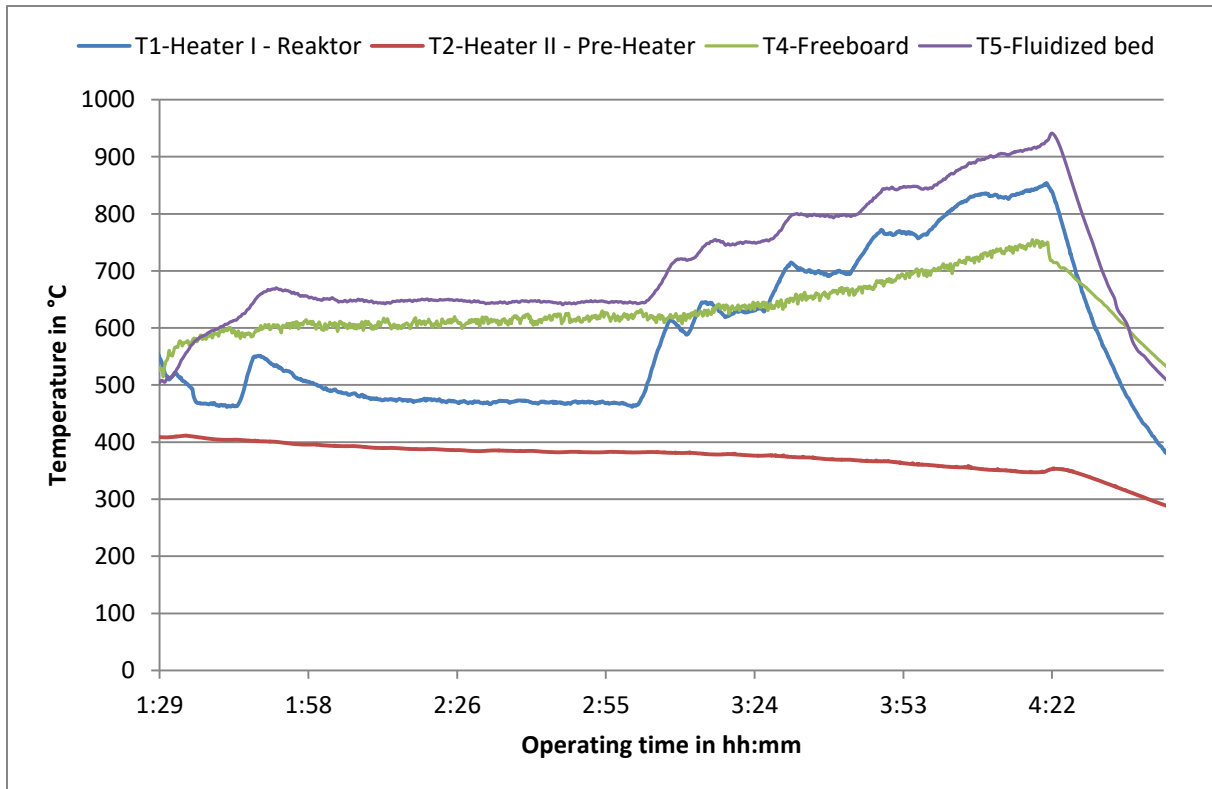


Figure 19: Temperature profile of lignin combustion in the lab-scale reactor

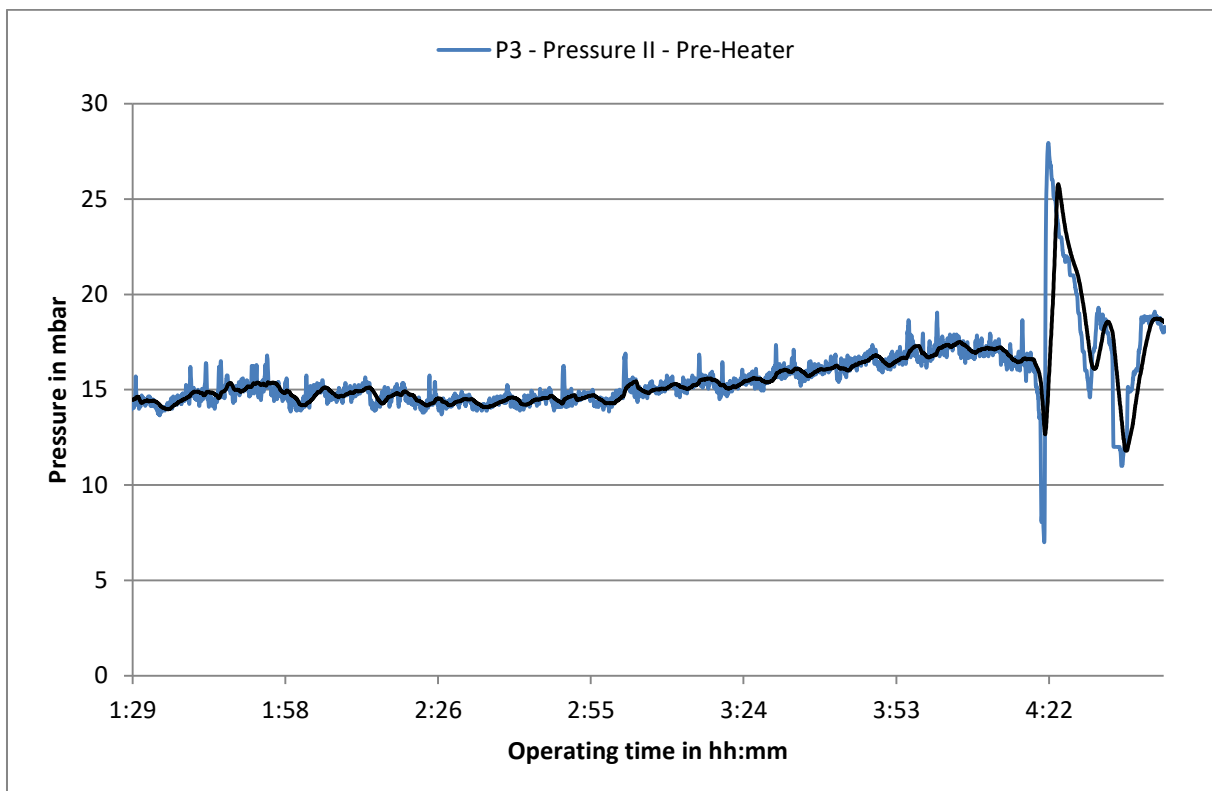


Figure 20: Pressure profile of lignin combustion in the lab-scale reactor

The reactor was cooled down, emptied and the samples of the bed material (right) and the coherent ash particles (left) were collected (Figure 21).



Figure 21: Combustion of lignin in the lab-scale reactor - Sample of the ash (left) and the bed material (right)

4.2. Bench-scale FB reactor

4.2.1. Wheat straw

During this campaign reactor walls have been preheated with electrical heaters prior to the start of fuel combustion at 1:35 (Figure 24). At approx. 4:00 the temperature at the splash zone, where combustion of the fuel takes place, reached 700 °C (Figure 22). Afterwards this temperature has been kept constant for several hours (ashing phase). Both electrical heaters (reactor and preheater) have been turned off and the ash content continuously increased. At 5:57, when the ash content reached approx. 10 wt.%, the ashing phase was terminated and the bed temperature has been continuously increased with the electrical heater. At 8:18, what corresponds to approximate 840 °C, the bed collapsed.

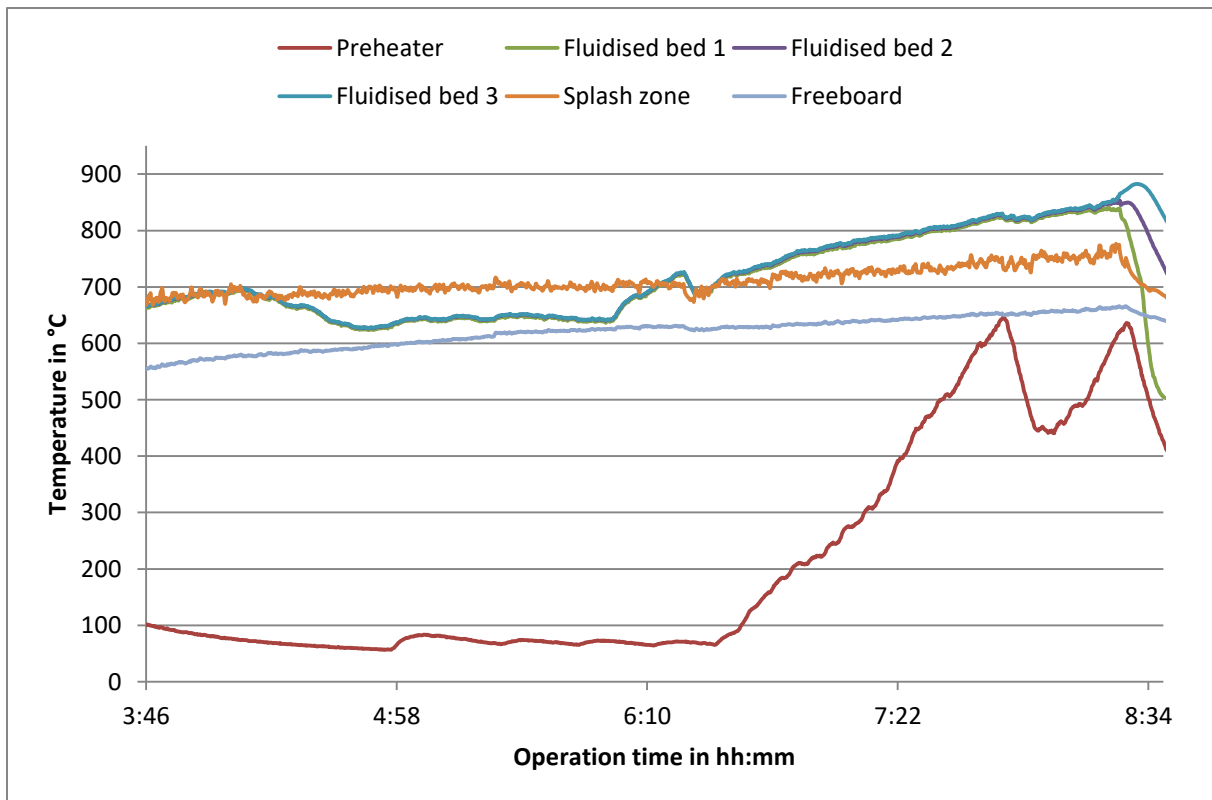


Figure 22: Temperature profile of wheat straw combustion in the bench-scale reactor

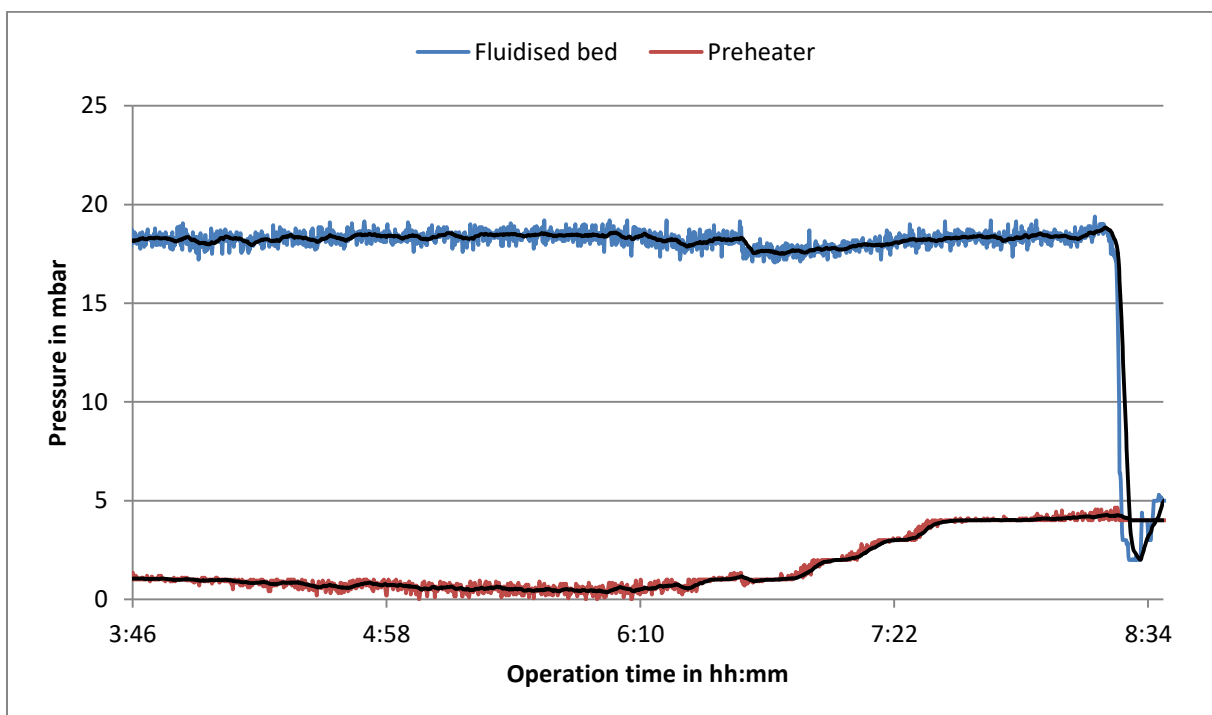


Figure 23: Pressure profile of wheat straw combustion in the bench-scale reactor

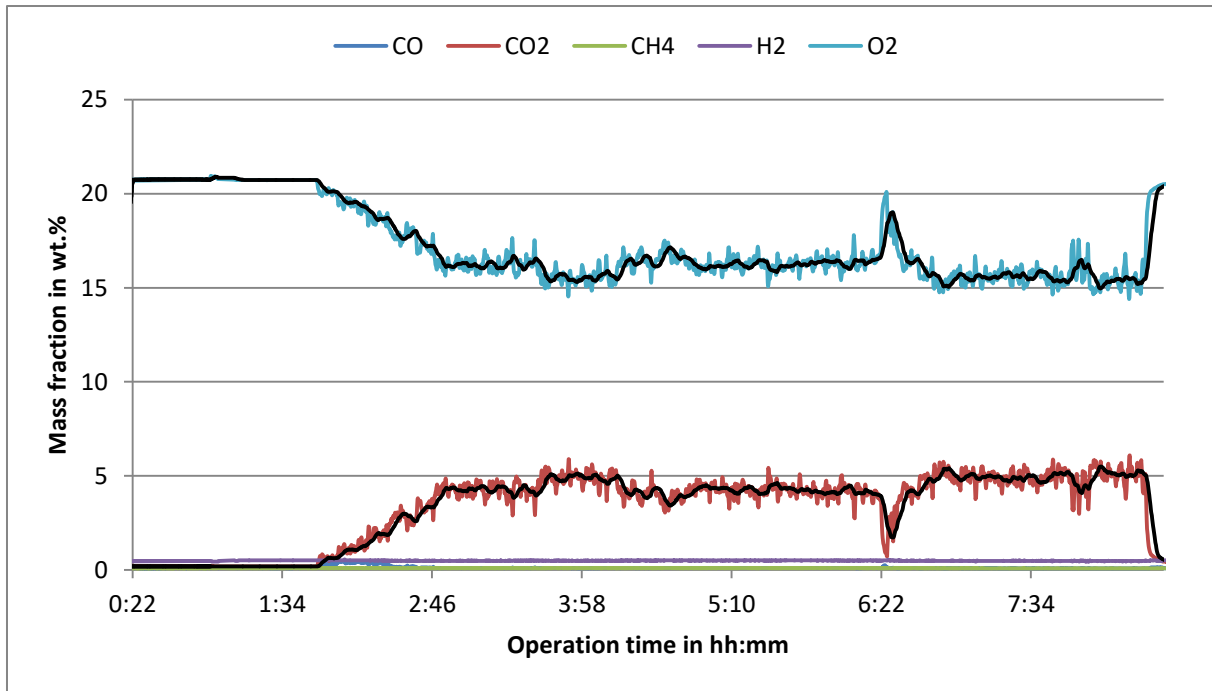


Figure 24: Composition profile of wheat straw combustion in the bench-scale reactor

The reactor was cooled down and the bed samples were collected. Figure 25 shows a glued bed material onto the reactors walls, probably through a melted ash.



Figure 25: Bench-scale reactor after experiment with wheat straw, deposit formation

4.2.2. Lignin

Due to interesting findings on the lignin ash behavior (formation of dimensionally stable ash residues, discussed later in 5.2), the focus of agglomeration investigation during this campaign was set on the influence of the feedstock preparation on their formation. Two experiments with pelletized and non-pelletized feedstock were conducted in the bench-scale reactor. Both experiments consisted only of the ashing phase, where the ash was produced at a constant temperature for approx. 3 hours at

700 °C. No incidents occurred during the operation. However, in the case of pelletized lignin, on- and off-fuel input was necessary in order to keep stable operation temperature (700 °C). Temperature profiles of the experiments are shown in Figure 26 and Figure 27. Afterwards, the ash samples were collected from the bed and visually examined (Figure 28 and Figure 29).

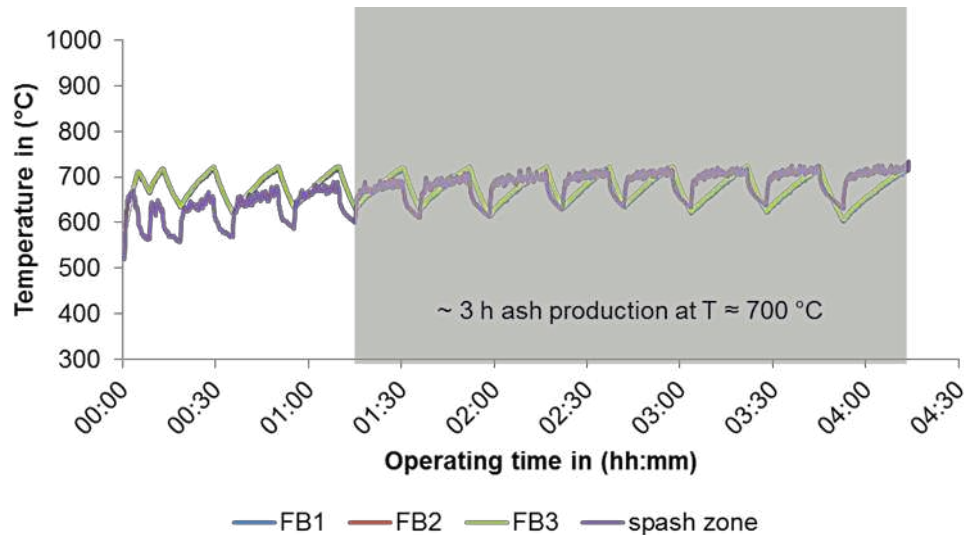


Figure 26: Combustion of pelletized lignin in the bench-scale reactor

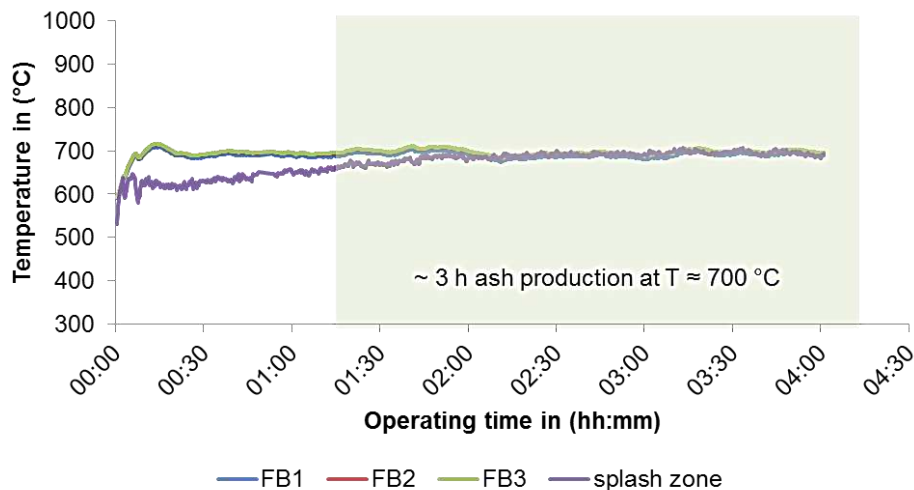


Figure 27: Combustion of non-pelletized lignin in the bench-scale reactor



Figure 28: Ash residues from the experiment with pelletized lignin



Figure 29: Ash residues from the experiment with non-pelletized lignin

4.3. 100kW DFB pilot-plant

The results shown in Figure 30 are adapted from a technical report on gasification of softwood and lignin. Lignin was gasified at two stable operation points: OP 2.1 at 830 °C and OP 2.2 at 800 °C.

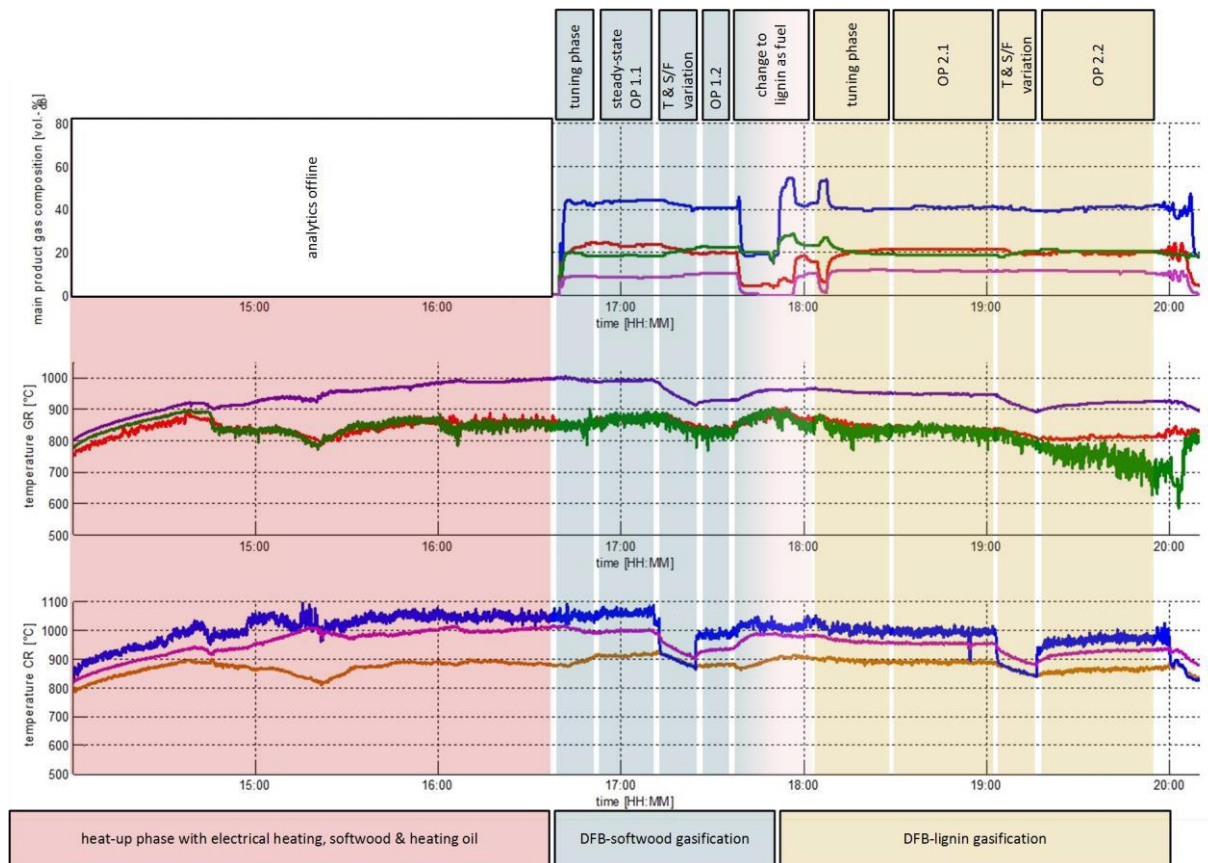


Figure 30: Temperature profile of lignin gasification in the 100kW DFB pilot-plant

During OP 2.1, no major issues occurred. The temperature was held constant between 800-850 °C (Figure 31) and at 19:00 the temperature was reduced to 800 °C (OP 2.2 - Figure 32). At approx. 19:15, the fluctuations in the bed temperature occurred (Figure 30– temperature GR, green line). Moreover the temperature of the upper part of the fluidized bed started to decrease. This depression continued till 20:00, when the experiment was terminated.

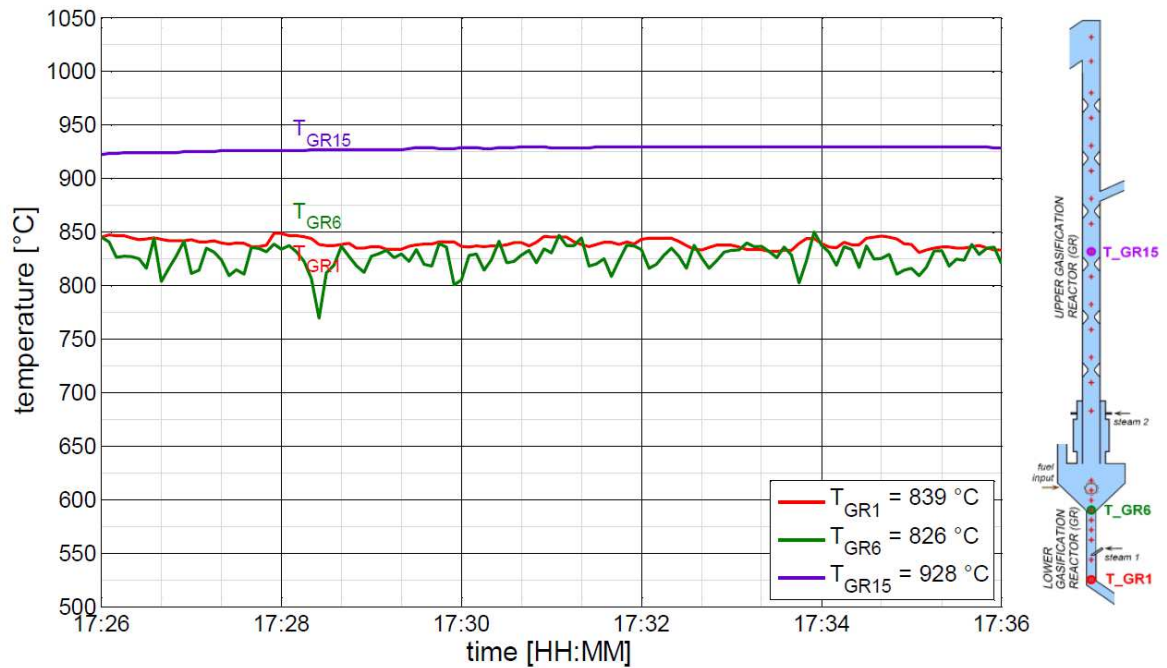


Figure 31: Temperature profile of lignin gasification in the 100kW DFB pilot-plant during operation point OP 2.1

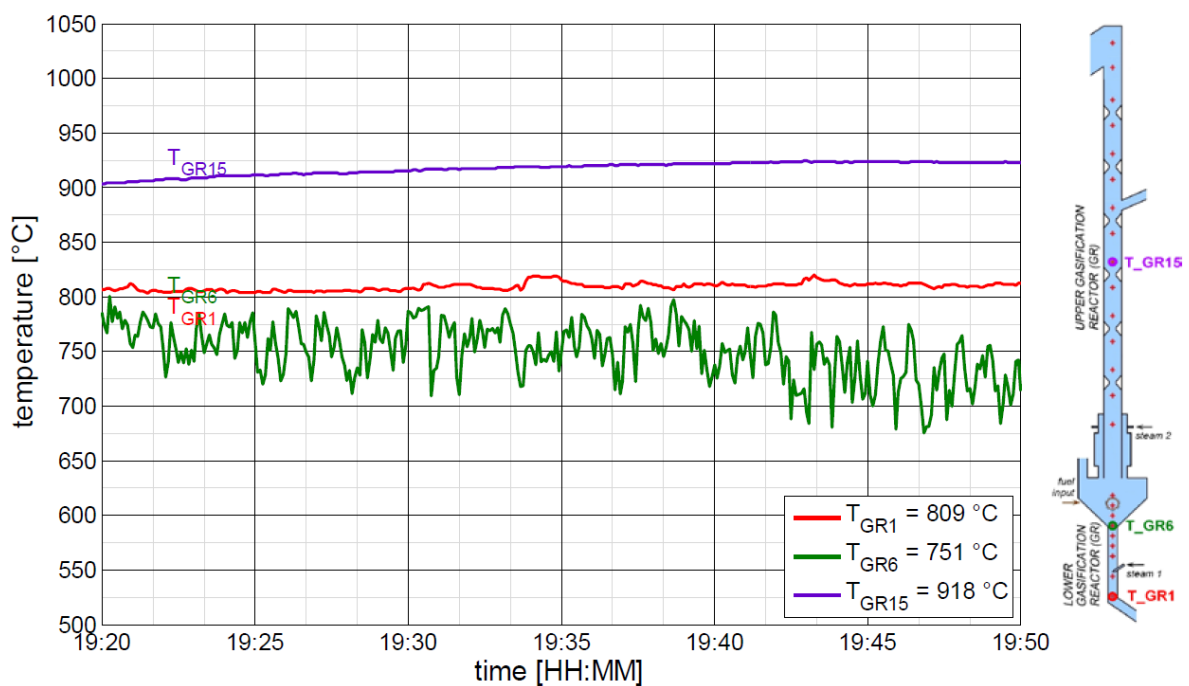


Figure 32: Temperature profile of lignin gasification in the 100kW DFB pilot-plant during operation point OP 2.2

Afterwards samples of dimensionally stable ash residues were collected from the bed and further examined. The ash composition of the collected ash residues together

with the composition of the feedstock ash (obtained by fuel analysis) is shown in Table 13. Carbon content of the ash residues is below 0.3 wt.%.

Table 13: Ash composition of the ash residues from the experiment in the 100kW DFB pilot-plant (Ash residues) and from the fuel analysis (Feedstock ash)

Oxid	Ash residues	Feedstock ash
Fe₂O₃	0.81%	0.71%
MnO	0.07%	0.07%
Cr₂O₃	0.08%	0.08%
TiO₂	0.13%	0.10%
CaO	3.45%	3.76%
K₂O	2.71%	3.08%
Cl	0.29%	0.58%
SO₃	0.24%	1.27%
P₂O₅	1.25%	1.23%
SiO₂	86.53%	84.46%
Al₂O₃	1.38%	2.62%
MgO	0.99%	0.35%
Na₂O	1.91%	1.48%

4.4. Equilibrium calculations in FactSage 7.2

4.4.1. Wheat straw

Figure 33 shows the chemical equilibrium calculations based on wheat straw composition at different temperatures at 1 atm. At 700 °C, first liquid phase (SLAGA#1) starts to form, composed mainly of SiO₂, P₂O₅, CaO, MgO and Na₂O (Figure 35). Its concentration stays practically constant till 840 °C, when it starts to increase, together with second liquid phase (SLAGA#2, Figure 36). The increase of both slags is accompanied by the decomposition of FTsalt, until its concentration reach the minimum at 920 °C. At this point, the fraction of the melted phase in the ash equals approx. 51 wt.% (Figure 34).

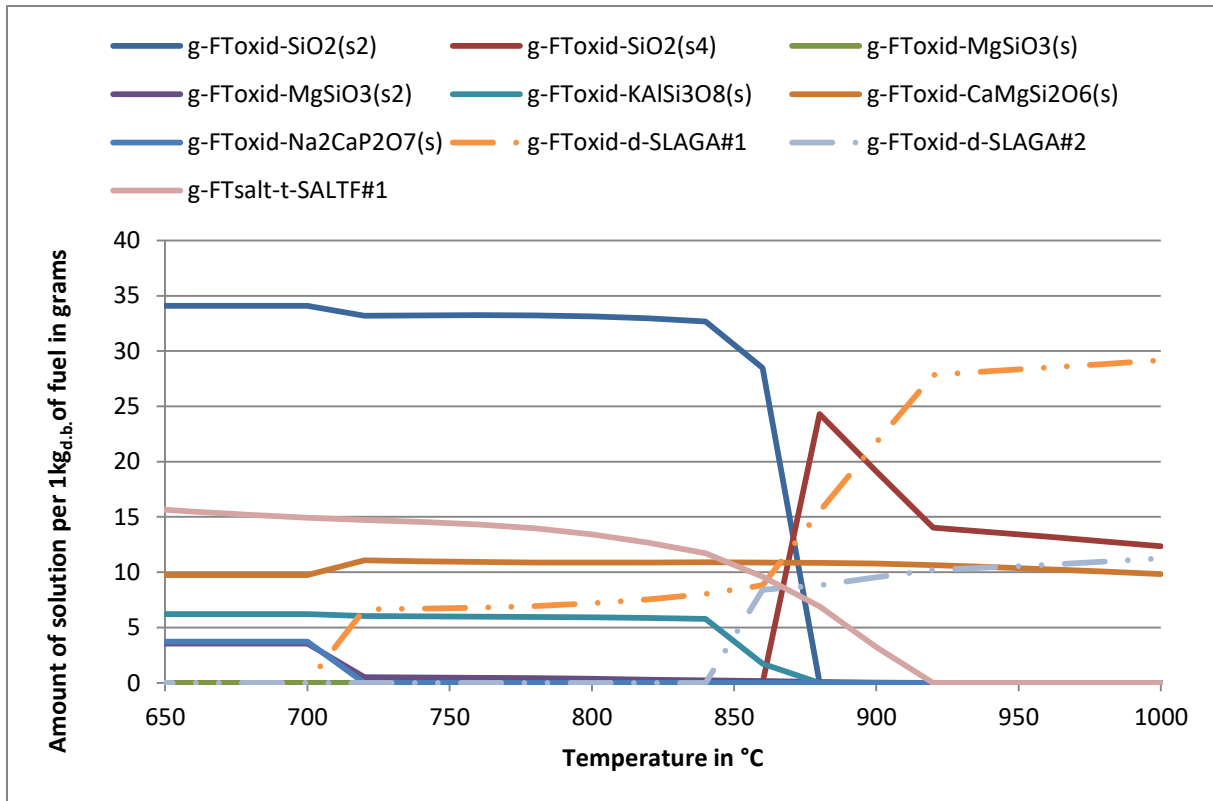


Figure 33: Chemical equilibrium based on the fuel composition of wheat straw

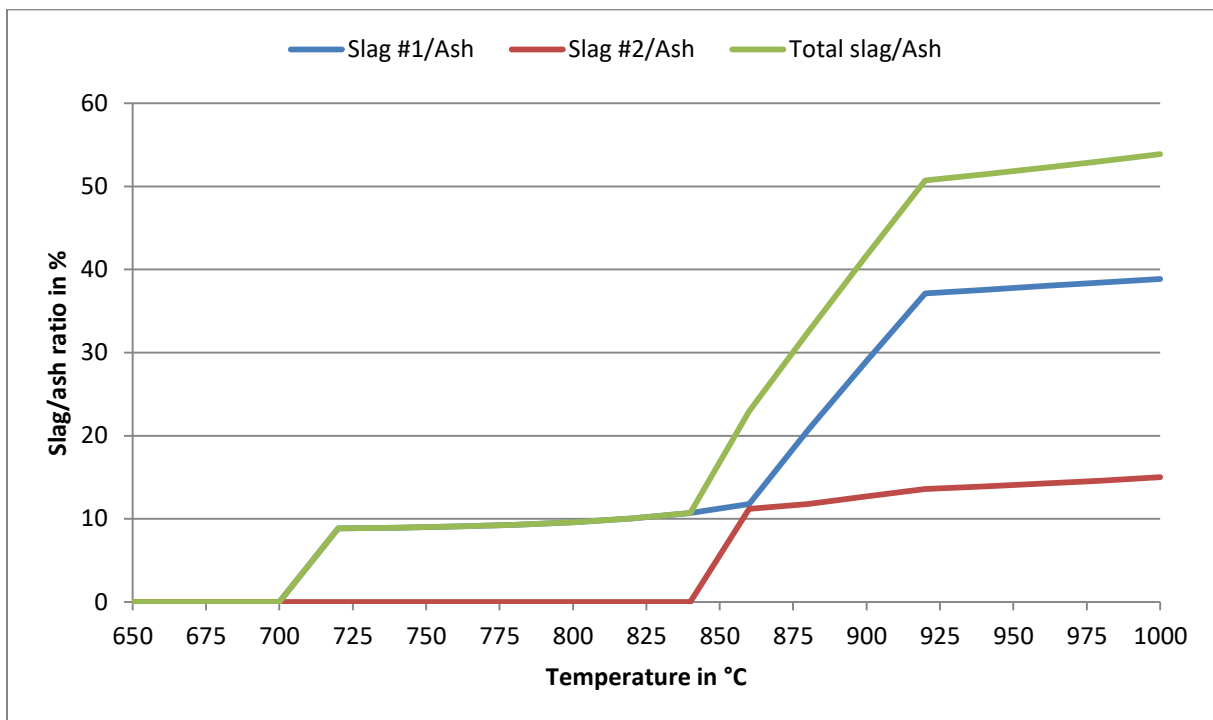


Figure 34: Fraction of melting phase in the ash of wheat straw

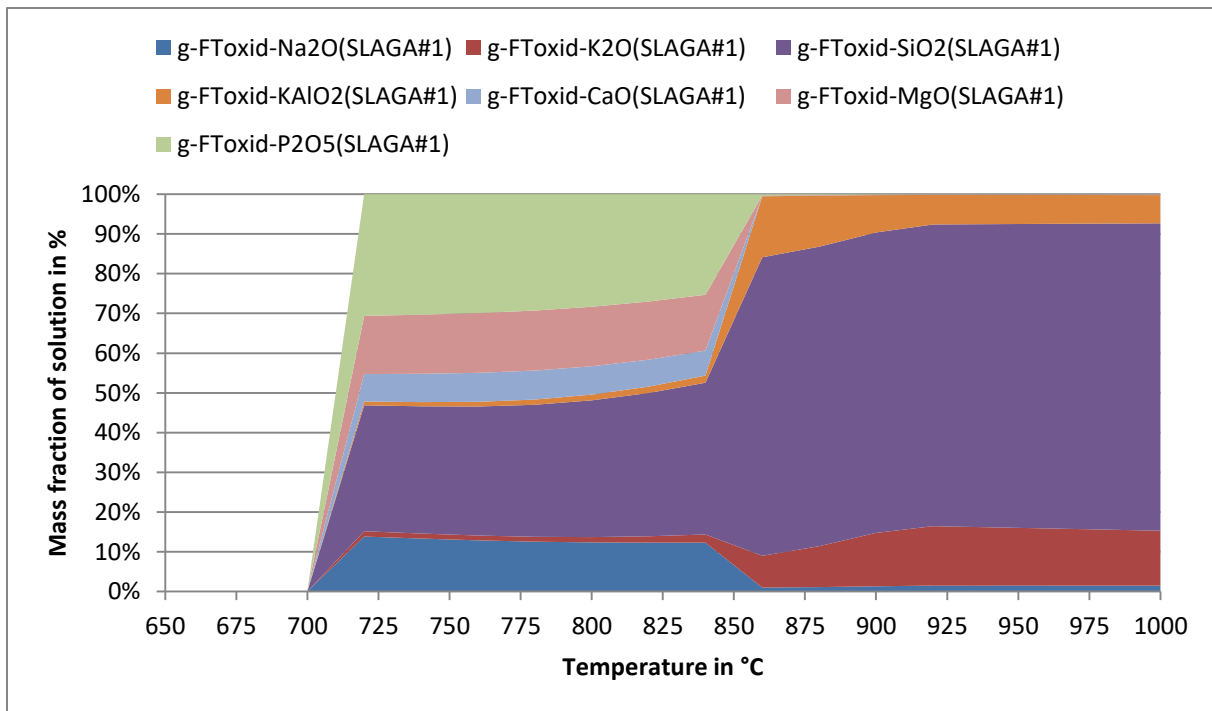


Figure 35: Composition of the SLAG#1 of wheat straw

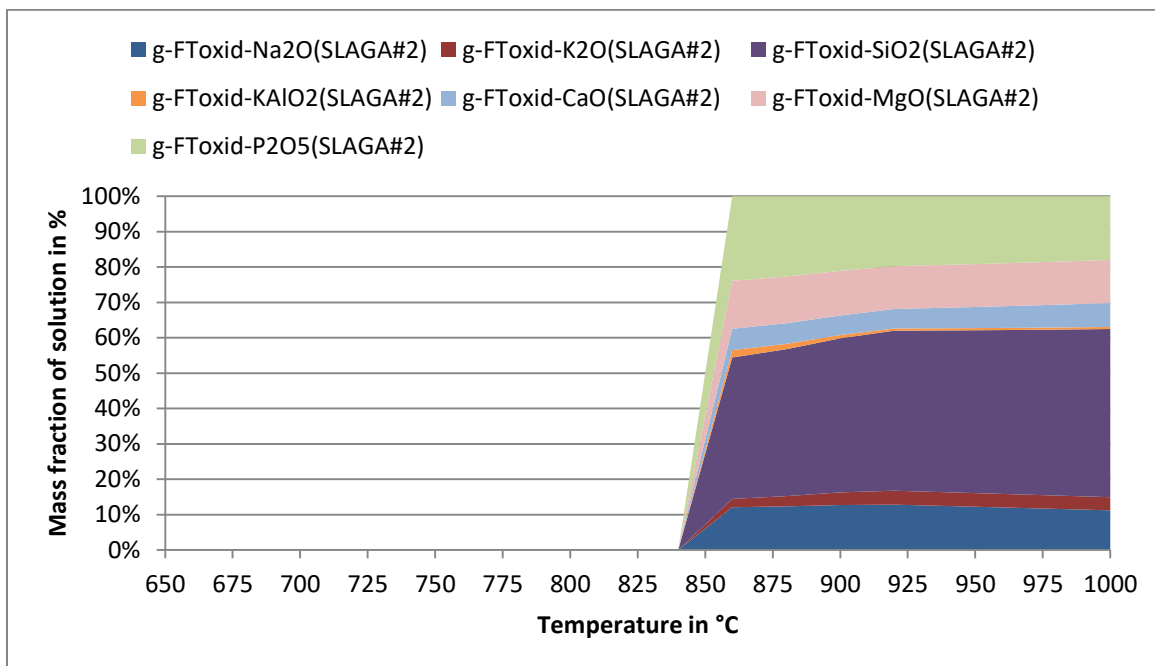


Figure 36: Composition of the SLAG#2 of wheat straw

Furthermore, a ternary diagram of the K_2O - CaO - SiO_2 has been examined and an eutectic point determined (Figure 37). Based on the ash composition (Table 9), concentration of CaO , K_2O and SiO_2 has been recalculated and normalized to 100%. Accordingly to Skoglund et.al [12], because of their similar behavior of the ash

transformation reactions, in such calculations Na_2O can be considered as K_2O . The same applies to MgO and CaO . There are 6 ternary compounds in this part of the system. Although none of those is known in nature, they are important to understand phase transformation of the system. Ash composition (marked in Figure 37 as a purple point) is situated inside subsystem $1:0:2$ ($\text{K}_2\text{O} \cdot 4\text{SiO}_2$) – $1:2:9$ ($\text{K}_2\text{O} \cdot 2\text{CaO} \cdot 9\text{SiO}_2$) – $1:0:4$ ($\text{K}_2\text{O} \cdot 4\text{SiO}_2$). Eutectic point is determined as an invariant point between these three phases. $\text{K}_2\text{O} \cdot 2\text{CaO} \cdot 9\text{SiO}_2$ is an example of an incongruently compound (upon heating it decomposes at a specific temperature to a liquid and another solid with different composition) and its primary phase composition (point $1:2:9$) lies outside the primary phase crystallization region (displayed with grey color). Therefore the eutectic temperature is approx. $700\text{ }^\circ\text{C}$ (Figure 37, red point) and corresponds to the lowest melting temperature of the subsystem.

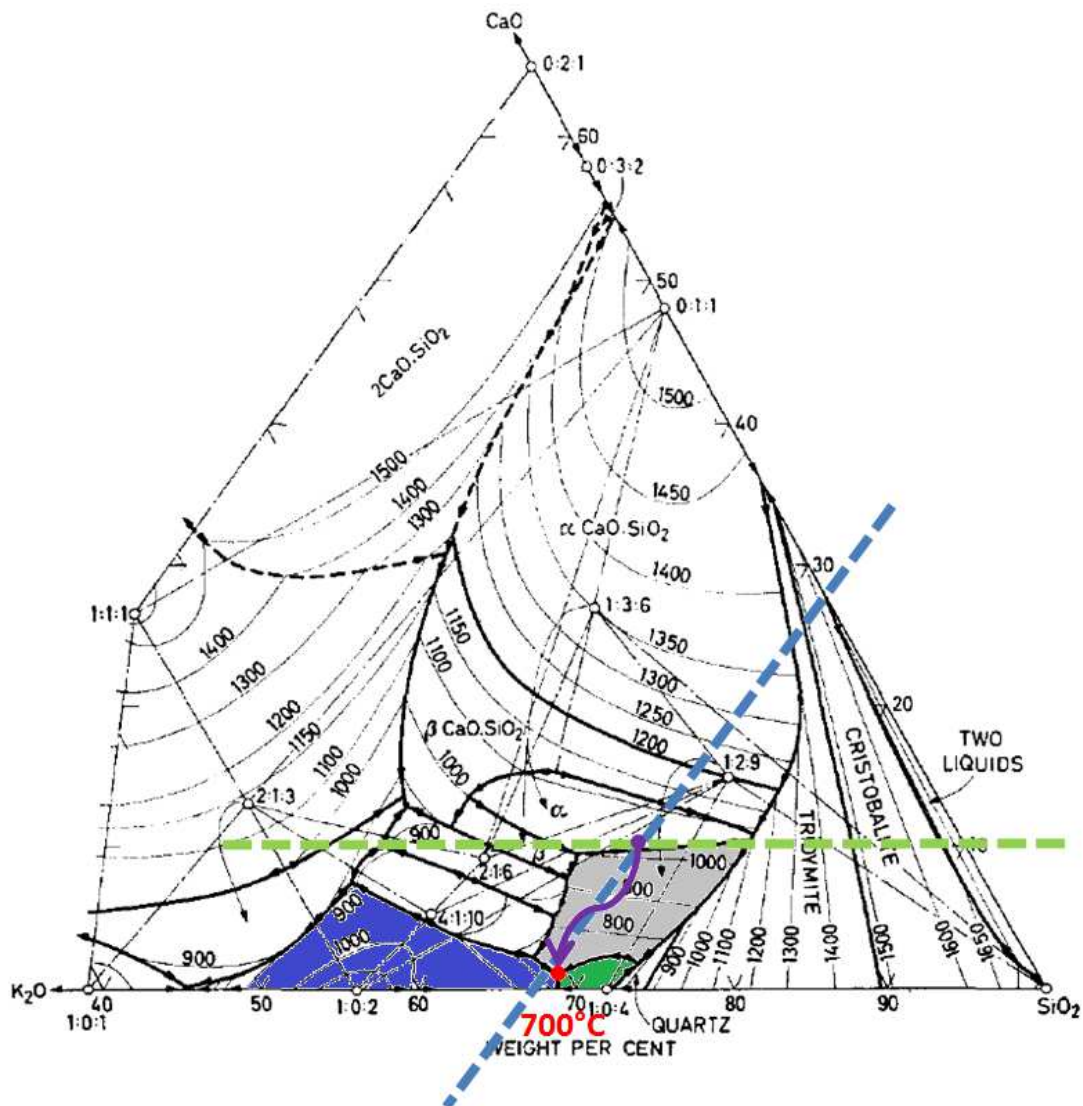


Figure 37: Part of a ternary phase diagram of the K_2O - CaO - SiO_2 system with an eutectic point at $700\text{ }^\circ\text{C}$

4.4.2. Lignin

As shown in Figure 38, first melt (SLAGA#1) starts to form at 770 °C, composed mainly of SiO_2 , Na_2O , P_2O_5 and CaO (Figure 39). At 850 °C, the amount of Slag#1 continues to increase, formed mainly from SiO_2 and alkali aluminates (Figure 39). SLAGA#2, consisting of SiO_2 , P_2O_5 , CaO and Na_2O starts to form at 840 °C (Figure 40). Figure 41 shows a fraction of melted phase in the ash. At its maximum at 950 °C, 33% of the ash is melted.

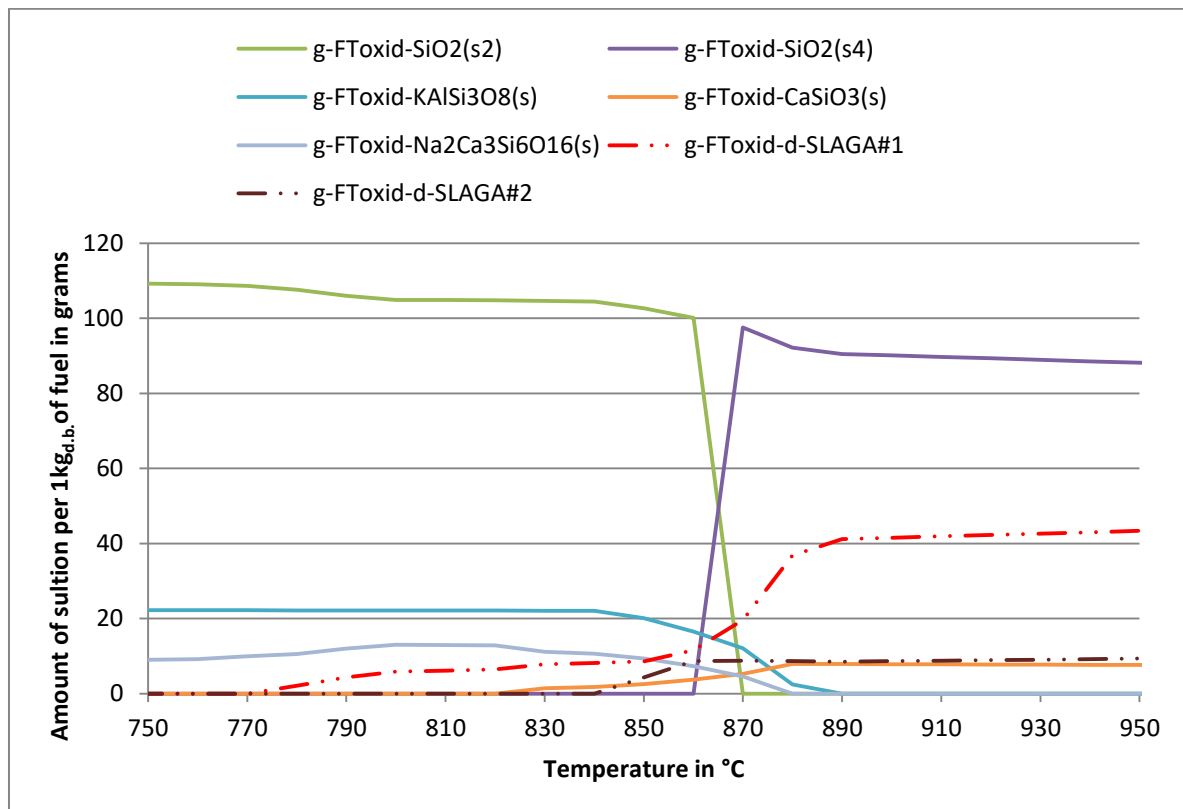


Figure 38: Chemical equilibrium based on fuel composition for lignin

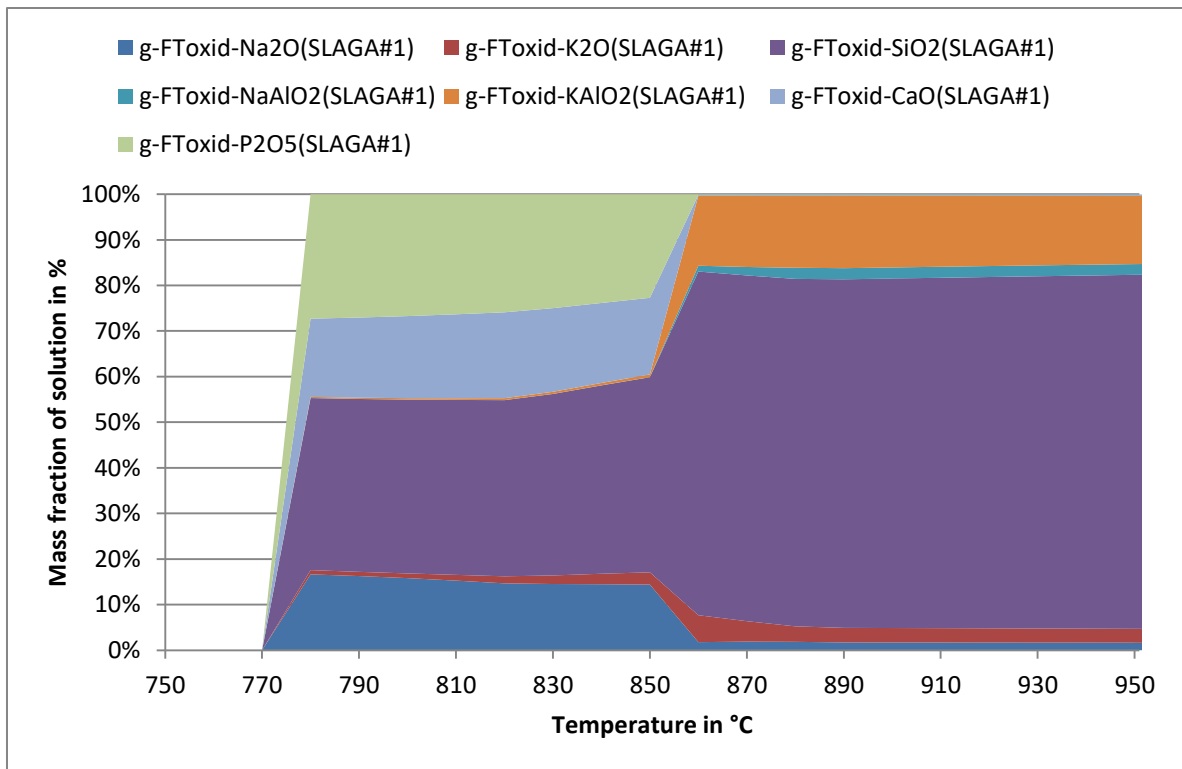


Figure 39: Composition of the SLAGA#1 for lignin

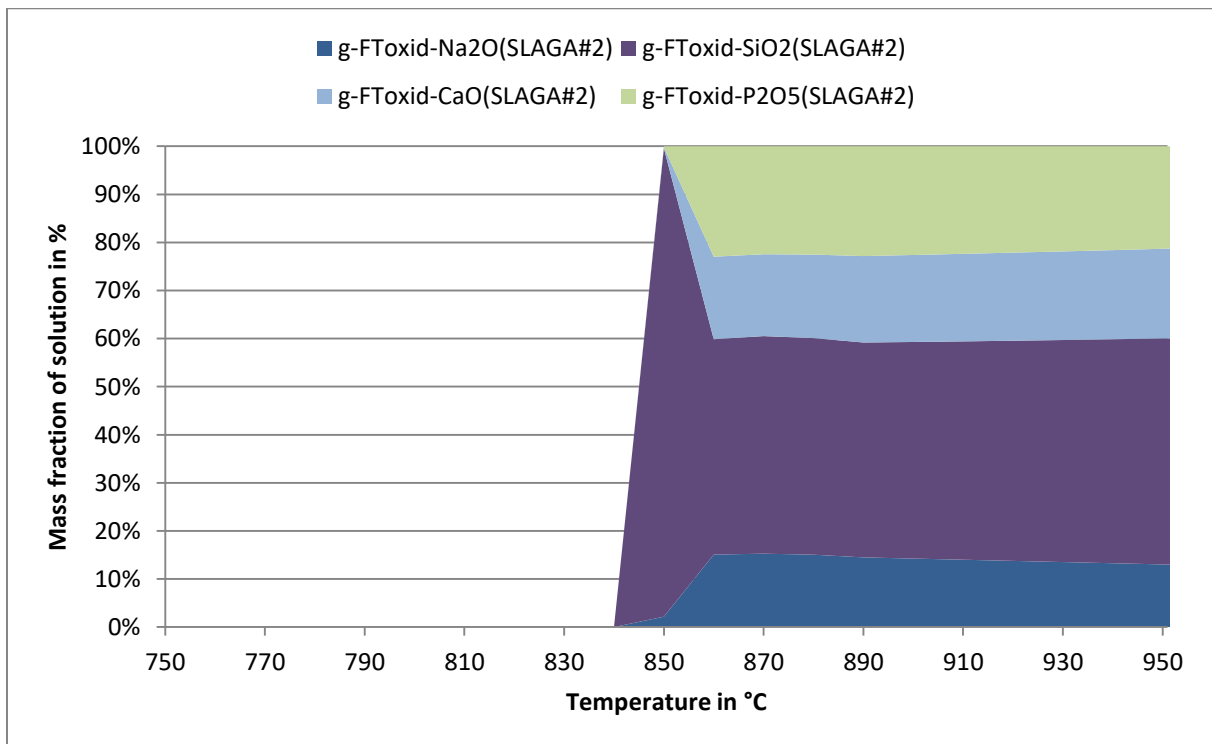


Figure 40: Composition of the SLAGA#2 for lignin

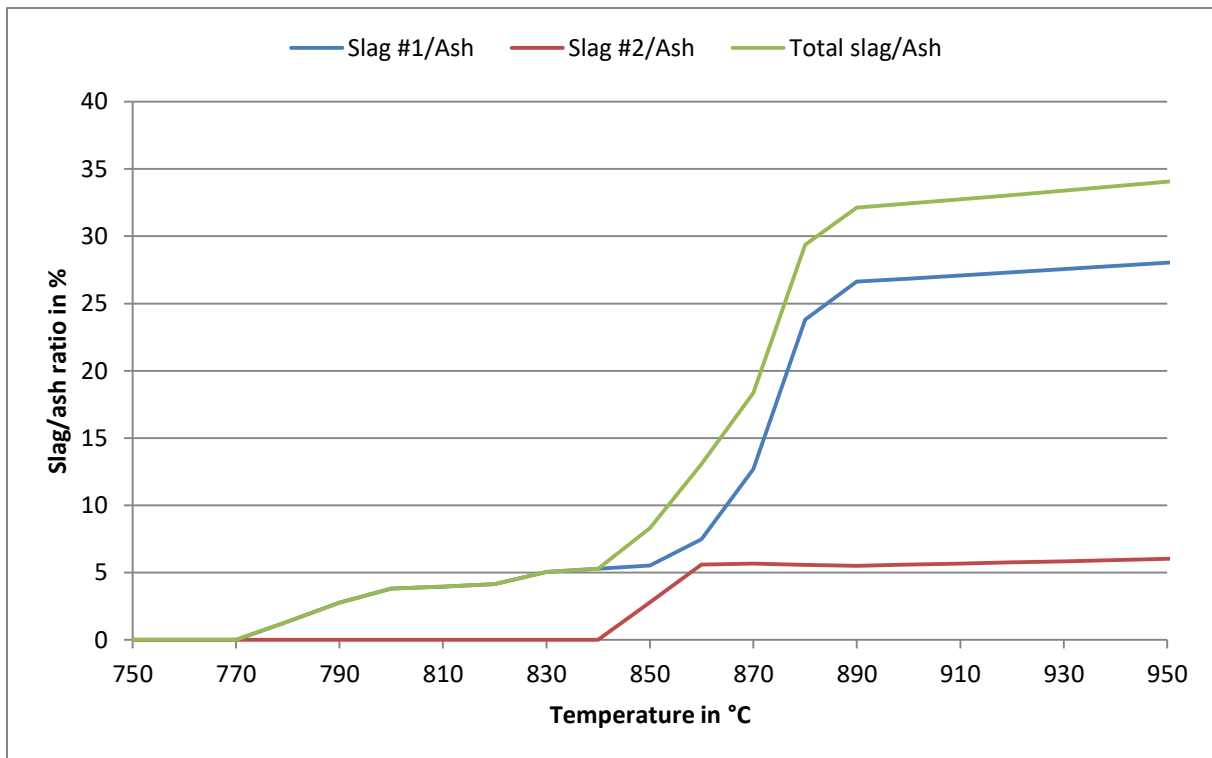


Figure 41: Fraction of melted phase in the lignin ash depending on temperature

Furthermore a ternary phase diagram of a system $\text{Na}_2\text{O}-\text{Al}_2\text{O}_3-\text{SiO}_2$ (Figure 42) has been chosen for comparison, since aluminium content in the lignin ash is considerably higher compared to the wheat straw (see Table 9). Similar to the previous chapter, the concentrations of Na_2O , SiO_2 and Al_2O_3 have been recalculated and normalized to 100%. Ash composition (marked in Figure 42 as a purple point) is situated inside subsystem 0:0:1 (SiO_2 - quartz) – 1:0:2 ($\text{Na}_2\text{O}\cdot 2\text{SiO}_2$ - natrosilite) – 1:1:6 ($\text{Na}_2\text{O}\cdot \text{Al}_2\text{O}_3\cdot 6\text{SiO}_2$ - albite) and therefore an eutectic temperature is approx. 740 °C (Figure 42, red point).

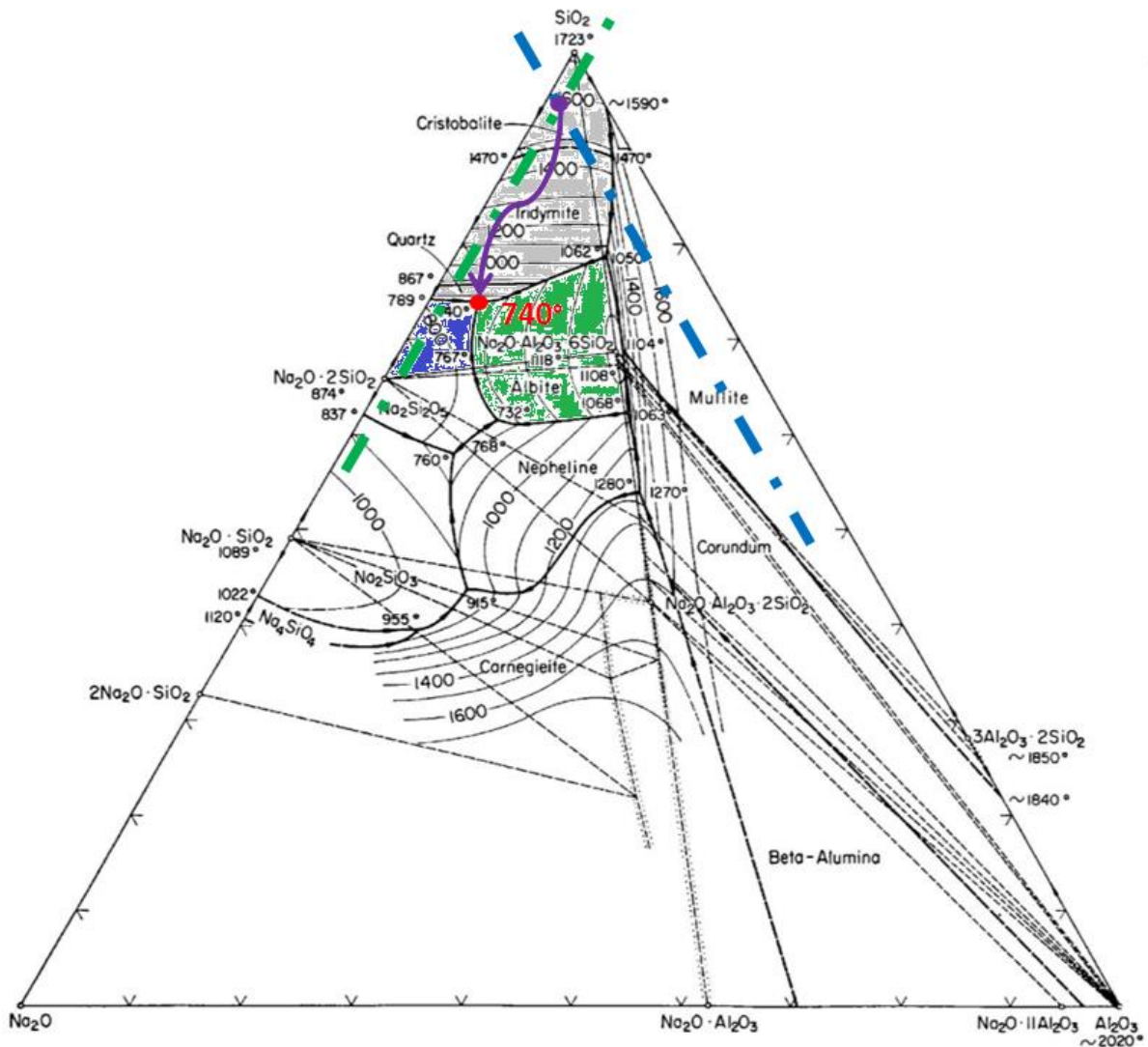


Figure 42: Ternary diagram of the Na₂O- Al₂O₃-SiO₂ system with an eutectic point at 740 °C

5. Discussion

5.1. Wheat straw

Thermodynamic equilibrium based on the ash composition (3.1.2) was calculated in Factsage7.2. Figure 33 shows, that first slag forms already at 700 °C. That is also in agreement with the interpretation of the K₂O-CaO-SiO₂ – system ternary diagram (Figure 37), where 700 °C corresponds to a eutectic temperature of the normalized ash. As can be seen in Figure 35 and Figure 36, sodium is becoming part of the melt

prior to potassium, what is in conflict with the reaction order, which was discussed in Chapter 2.3.1. This is probably caused by the absence of some potassium phosphates (e.g. KPO_3) in the Factsage database. However, as already mentioned in Chapter 4.4.1, potassium and sodium play a similar role in the ash transformation reactions and consequently, the inversed formation order should not have an impact on the total slag amount.

The experiments with wheat straw were performed in the lab-scale and the bench-scale reactor. In both cases, the experiments ended up with a bed collapse caused by bed agglomeration. The agglomeration temperatures were determined to be 865 °C in the lab-scale (4.1.1), and 840 °C in the bench-scale reactor (4.2.1). The difference was probably caused by a higher heating rate in the case of the lab-scale reactor - since the amount of bed material in the lab-scale reactor is approx. 10x lesser compared to the bench-scale reactor, it is more difficult to maintain a consistent increase of the bed temperature. However, both experimentally obtained agglomeration temperatures exceed the temperature predicted with equilibrium calculations (4.4.1) by 140 °C. Hence, these calculations are not suitable for prediction of the agglomeration temperature, since the system in the reactor during combustion is far from the equilibrium. That can be caused by the fact, that calculations are based on complete availability of each element for the reaction, which is not possible in the real system because of their non-uniform distribution in the ash particle. Moreover, the amount of alkali metals (which have a major effect on the agglomeration temperature) available for the reactions, is considerably lower during fluidized bed combustion. This is caused by the fact, that Factsage doesn't take into account the carrying out of the alkali metals, which are partly released to the gas phase already at 726 °C [27].

Furthermore the bed material was after the experiments collected and visually examined. During the unsuccessful experiment with 50 grams of the bed material no agglomeration was detected neither by pressure sensors nor thermocouples (4.1.1). However after the bed was cooled down, single large agglomerate with a diameter of 5 cm and height of 3 cm (Figure 18) was found in the reactor, glued to the reactor walls above the bed. Beneath was bed material unaffected by agglomeration. That was probably caused by high ash content (over 50 wt.%) in comparison to the

amount of the bed material. The ash accumulated at the top of the bed due to its density and melted, creating the agglomerate, which prevented further contact between the bed material and the fuel particles.

The other experiment in the lab-scale reactor with 300 g of the bed material already provided the information about the wheat straw agglomeration temperature: the thermocouples (Figure 15) as well as the pressure sensor (Figure 16) detected the agglomeration start (840 °C). This temperature is in good agreement with the chemical equilibrium calculations, since it matches the start of the formation of SLAGA#2 (Figure 33).

The experiment in the bench-scale reactor also ended up due to agglomeration. As can be seen in Figure 22 and Figure 23, both thermocouples and pressure sensors clearly detected a bed collapse at 840 °C. After the bed was cooled down and released, it was found, that some of the bed material was glued by the molten ash onto the reactor walls (Figure 25). Although this agglomerated bed material comprised only a small fraction of its total amount, it was still sufficient for total defluidisation.

5.2. Lignin

The start of the slag formation based on the XRF analysis of the fuel was calculated using Factsage 7.2 (4.4.2). This temperature appears to be valid, since the temperature for a melt formation of a ternary eutectic in the subsystem silica–albite–sodium disilicate in $\text{SiO}_2\text{-Na}_2\text{O-Al}_2\text{O}_3$ system (Figure 42) is situated at 740 °C [28].

However none of the experiments in the lab-scale, bench-scale and pilot-plant reactor ended up due to agglomeration (see chapters 4.1.2, 4.2.2 and 4.3). A possible reason could be a low fraction of the molten phase, which represents only 5% of the total ash amount at the operation temperatures. It has been observed, that in order for the particle to be sticky, the fraction of the molten phase needs to be at least 15% [29]. Consequently, the agglomeration will not occur during lignin combustion.

However, partial melting could be a reason for another phenomenon observed during the experiment: formation of dimensionally stable ash residues, so called skeleton

particles. These particles have been first observed during the experiment in the lab-scale reactor (chapter 4.1.2). After approx. 3 hours of combustion, the pressure sensor detected sudden defluidisation of the bed (Figure 20). The defluidisation was caused by dimensionally stable ash particles, which were found in the reactor after the experiment (Figure 21). It appears that these ash particles accumulate at the top of the bed, forming a dense layer (Figure 43). At a certain height, this layer can cause pressure and temperature fluctuations in the bed or eventually defluidisation.

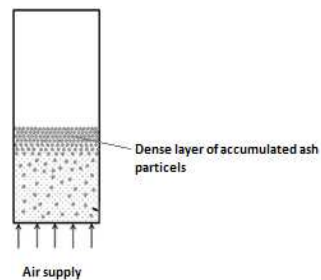


Figure 43: Formation of the dense particle layer on the top of the bed

The formation of these particles is illustrated in Figure 44. In the case of e.g. softwood pellets after the volatiles are released (a1-a2), the char particles (a2) are transformed into smaller ash particles via combustion (a2-a3). These ash particles are afterwards partly carried out from the bed with the fluidizing medium (air) as a fly ash. Formation of the lignin char particles is analogous to softwood (b1-b2). However, unlike the softwood char, the lignin char does not disintegrate into smaller ash particles, but retains its original shape (b2-b3). As a result, these dimensionally stable ash residues remain in the bed, forming the above mentioned dense layer.

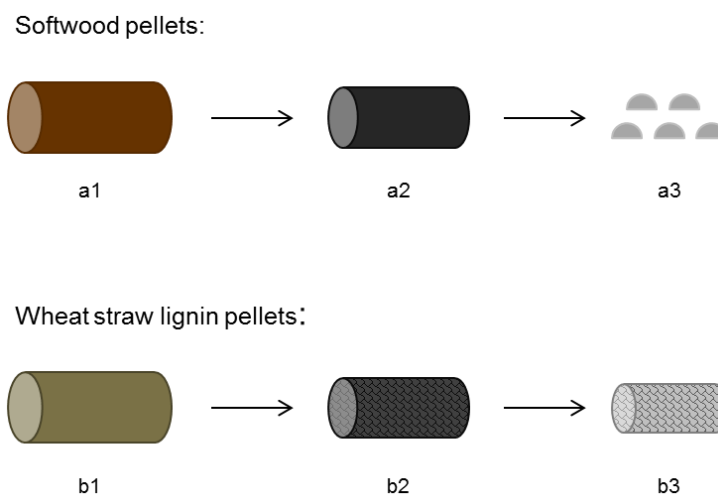


Figure 44: Formation of the softwood and the lignin ash

In order to compare the formation of the dimensionally stable ash residues between pelletized and non-pelletized lignin, additional experiments were performed in the bench-scale reactor (both experiments are described in chapter 4.2.2). Visual examination of the samples from both beds shows significant differences between these two feedstocks. Combustion of the non-pelletized feedstock resulted in the formation of less stable ash residues with cracks along the layers of the lignin plates (Figure 29). These cracks probably cause higher attrition of the skeleton particle, resulting in their lesser accumulation on the top of the bed. The crack formation is illustrated in Figure 45.

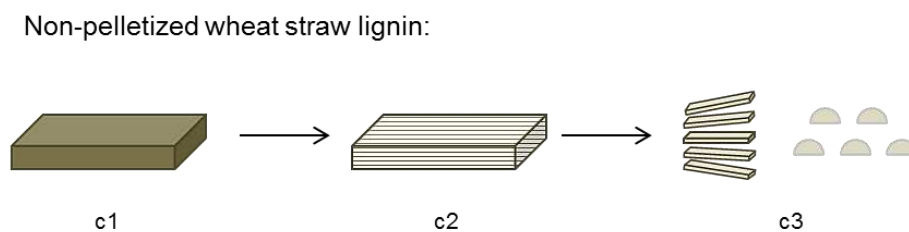


Figure 45: Crack formation on the non-pelletized lignin particle

On the other hand, combustion of pelletized feedstock leads to the formation of more stable skeleton particles (Figure 28). The surface of these particles is smooth and in contrast to non-pelletized feedstock, no visible cracks occur. That is probably caused by the pelletizing process, in which the particle strength and density is being enhanced under mechanical pressure and elevated temperature (3.1.1). The pelletizing process also improves solid-solid contacts inside the particle, increasing its thermal conductivity [30], which can lead to a more extensive local overheating. Moreover the increase in solid-solid contacts considerably improves the probability of reactions among the ash-forming elements, leading to more intensive slag formation.

5.3. Suitability of the reactors for agglomeration tests

The new method for agglomeration determination, which was proposed in chapter (Fehler! Verweisquelle konnte nicht gefunden werden.), was tested in the lab-scale and the bench-scale reactor with wheat straw and lignin.

The results show, that both reactors demonstrated the suitability for determination of the melt-induced agglomeration (2.4.2). However, in comparison to the bench-scale reactor, the lab-scale reactor has certain disadvantages. First, the incapability of collecting an ash or a bed material sample during the experiment is problematic in the lab-scale reactor. In order to collect the sample, the reactor needs to be first cooled down and opened. Another significant disadvantage is a sensitive response to any change in the operation, such as increasing/decreasing the air flow or adjusting the heaters power or the fuel input. It has been observed, that only a small change in these parameters leads to great fluctuations of the bed pressure and temperature. Furthermore the lab-scale reactor lacks both a cyclone and a secondary bunker, what rules out the opportunity to examine coating-induced agglomeration. On the other hand, smaller dimensions and a more simply set-up of the bench scale reactor allows easier handling of the apparatus and significantly lower preparation time.

In the 100kW DFB pilot-plant examination of both, melt -and coating-induced agglomeration mechanisms is possible. However, a great amount of time, necessary for removing the molten ash and bed material residues from the reactor makes it unsuitable for studying the melt-induced agglomeration.

5.4. Comparison of methods for determination of ash behavior in FB reactor

Table 14 shows comparison of the ash melting temperatures acquired by the standard ASTM fusion test (Table 8 - IDT), equilibrium calculations in Factsage (4.4.1; 4.4.2) and the experiments in the lab-scale FB reactor (4.1.1; 4.1.2).

Table 14: Comparison of ash melting temperatures from the ASTM test, equilibrium calculations and the lab-scale FB reactor test

	Wheat Straw	Lignin
ASTM	830 °C	1430 °C
Factsage	700 °C	770 °C
FB reactor	840- 865 °C*	900 °C

*lab-scale/bench-scale FB reactor

In the case of wheat straw, the initial deformation temperature IDT determined by the ASTM test is comparable with agglomeration temperature obtained from the experiments in the both FB reactors, at which bed particles adhere together due to molten ash (so called “melt-induced” agglomeration). However, as already established by several authors, the ASTM fusion test fails to predict the

agglomeration temperature in most cases, since the interactions between ash particles and bed material are excluded from the test. These interactions lead to a formation of a uniform coating on the bed material surface, which at elevated temperatures may initiate agglomeration (“coating-induced agglomeration”). On the other hand, the method proposed by Öhman and Nordin [20] is suitable for determination of both agglomeration types. However it may not be able to detect other problematic ash behavior – formation and accumulation of the coherent ash particles in the fluidized bed. In order to detect such problematic ash behavior, an inclusion of burning char particles as well as progressive accumulation of ash in the bed in the used method is necessary. Such method has been proposed and tested with wheat straw and wheat straw lignin. The developed method is capable to determine the bed agglomeration temperature, as well as formation and accumulation of coherent ash particles.

6. Conclusion

The aim of this thesis was to develop a new reliable method for determination of agglomeration during fluidized bed combustion, which should besides ash-bed material interactions also account for the influence of local overheating caused by burning char particles.

Such a method was proposed and tested in the lab-scale and bench-scale reactor with two different fuels: wheat straw and wheat straw lignin. The experiments with wheat straw proved the applicability of the method in the fluidized bed system. Melt-induced agglomeration has been detected in both, lab-scale and bench-scale reactors, and the agglomeration temperatures have been determined. They appear to be in good agreement with the results of chemical equilibrium calculations, performed in Factsage 7.2.

During lignin combustion in the lab-scale reactor, an accumulation of dimensionally stable ash residues (skeleton particles) at the top of the bed has been observed. This phenomenon was further examined in the bench-scale reactor. In the bench-scale reactor, both pelletized and non-pelletized feedstock has been used. Results show,

that combustion of pelletized lignin leads to a larger accumulation of these particles at the top of the reactor. A possible explanation has been offered in chapter 5.2. Behavior of lignin in gasification conditions has been further investigated in 100kW DFB pilot-plant. Similar to the experiments in the lab-scale and the bench-scale reactor, formation of the coherent ash residues, which led to a pressure and temperature fluctuation, has been reported.

References

- [1] S.C. Davis, W. Hay, J. Pierce, Biomass in the energy industry: An introduction, Lond. GB BP Plc. (2014).
- [2] H. Hofbauer, R. Rauch, K. Bosch, R. Koch, Ch. Aichernig, Biomass CHP Plant Güssing – A Success Story, (n.d.) 13.
- [3] L.E. Fryda, K.D. Panopoulos, E. Kakaras, Agglomeration in fluidised bed gasification of biomass, Powder Technol. 181 (2008) 307–320. doi:10.1016/j.powtec.2007.05.022.
- [4] A. UNFCCC, 8, Clarifications on definition of biomass and consideration of changes in carbon pools due to a CDM project activity, EB. 20 (n.d.) 1.
- [5] A. Demirbaş, Biomass resource facilities and biomass conversion processing for fuels and chemicals, Energy Convers. Manag. 42 (2001) 1357–1378. doi:10.1016/S0196-8904(00)00137-0.
- [6] J.L. Easterly, M. Burnham, Overview of biomass and waste fuel resources for power production, Biomass Bioenergy. 10 (1996) 79–92. doi:10.1016/0961-9534(95)00063-1.
- [7] D. Mohan, Pittman Charles U., P.H. Steele, Pyrolysis of Wood/Biomass for Bio-oil: A Critical Review, Energy Fuels. 20 (2006) 848–889. doi:10.1021/ef0502397.
- [8] P. Basu, Biomass Gasification and Pyrolysis: Practical Design and Theory, Academic Press, 2010.
- [9] M. Kolbitsch, First fuel tests at a novel 100 kWth dual fluidized bed steam gasification pilot plant, TU Wien Dr. Thesis. (2016).
- [10] T. Nussbaumer, Combustion and Co-combustion of Biomass: Fundamentals, Technologies, and Primary Measures for Emission Reduction, Energy Fuels. 17 (2003) 1510–1521. doi:10.1021/ef030031q.
- [11] D. Boström, N. Skoglund, A. Grimm, C. Boman, M. Öhman, M. Broström, R. Backman, Ash Transformation Chemistry during Combustion of Biomass, Energy Fuels. 26 (2012) 85–93. doi:10.1021/ef201205b.
- [12] N. Skoglund, Umeå universitet, Tillämpad fysik och elektronik, Ash chemistry and fuel design focusing on combustion of phosphorus-rich biomass, Department of applied physics and electronics, Umeå universitet, 2014.
- [13] B. Gatterig, J. Karl, Investigations on the Mechanisms of Ash-Induced Agglomeration in Fluidized-Bed Combustion of Biomass, Energy Fuels. 29 (2015) 931–941. doi:10.1021/ef502658b.
- [14] K. Wagner, M. Kuba, G. Häggström, N. Skoglund, M. Öhman, H. Hofbauer, Influence of Phosphorus on the Layer Formation on K-feldspar During Fluidized Bed Combustion and Gasification, Eur. Biomass Conf. Exhib. Proc. 26th EUBCE-Copenhagen 2018 (2018) 486–492. doi:10.5071/26thEUBCE2018-2BO.6.2.
- [15] H. He, X. Ji, D. Boström, R. Backman, M. Öhman, Mechanism of Quartz Bed Particle Layer Formation in Fluidized Bed Combustion of Wood-Derived Fuels, (2016). doi:10.1021/acs.energyfuels.5b02891.
- [16] M. Öhman, A. Nordin, B.-J. Skrifvars, R. Backman, M. Hupa, Bed Agglomeration Characteristics during Fluidized Bed Combustion of Biomass Fuels, Energy Fuels. 14 (2000) 169–178. doi:10.1021/ef990107b.

- [17] H. He, N. Skoglund, M. Öhman, Time-Dependent Crack Layer Formation in Quartz Bed Particles during Fluidized Bed Combustion of Woody Biomass, *Energy Fuels*. 31 (2017) 1672–1677. doi:10.1021/acs.energyfuels.6b02980.
- [18] M. Kuba, H. He, F. Kirnbauer, N. Skoglund, D. Boström, M. Öhman, H. Hofbauer, Mechanism of Layer Formation on Olivine Bed Particles in Industrial-Scale Dual Fluid Bed Gasification of Wood, *Energy Fuels*. 30 (2016) 7410–7418. doi:10.1021/acs.energyfuels.6b01522.
- [19] B.-J. Skrifvars, M. Öhman, A. Nordin, M. Hupa, Predicting Bed Agglomeration Tendencies for Biomass Fuels Fired in FBC Boilers: A Comparison of Three Different Prediction Methods, *Energy Fuels*. 13 (1999) 359–363. doi:10.1021/ef980045+.
- [20] M. Öhman, A. Nordin, A New Method for Quantification of Fluidized Bed Agglomeration Tendencies: A Sensitivity Analysis, *Energy Fuels*. 12 (1998) 90–94. doi:10.1021/ef970049z.
- [21] F. Scala, Particle agglomeration during fluidized bed combustion: Mechanisms, early detection and possible countermeasures, *Fuel Process. Technol.* 171 (2018) 31–38. doi:10.1016/j.fuproc.2017.11.001.
- [22] N. Kaliyan, R. Vance Morey, Factors affecting strength and durability of densified biomass products, *Biomass Bioenergy*. 33 (2009) 337–359. doi:10.1016/j.biombioe.2008.08.005.
- [23] W. Stelte, C. Clemons, J.K. Holm, J. Ahrenfeldt, U.B. Henriksen, A.R. Sanadi, Fuel Pellets from Wheat Straw: The Effect of Lignin Glass Transition and Surface Waxes on Pelletizing Properties, *BioEnergy Res.* 5 (2012) 450–458. doi:10.1007/s12155-011-9169-8.
- [24] D. Eßletzbichler, Auslegung, Aufbau und Inbetriebnahme einer Wirbelschichtapparatur im Labormaßstab für thermische Umwandlungsprozesse von Biomasse, (2017) 161.
- [25] F. Benedikt, A.M. Mauerhofer, J. Fuchs, J.C. Schmid, Gasification of Softwood and Lignin, Technical Report of Scientific Research, (2018).
- [26] C.W. Bale, E. Bélisle, P. Chartrand, S.A. Decterov, G. Eriksson, A.E. Gheribi, K. Hack, I.-H. Jung, Y.-B. Kang, J. Melançon, A.D. Pelton, S. Petersen, C. Robelin, J. Sangster, P. Spencer, M.-A. Van Ende, FactSage thermochemical software and databases, 2010–2016, *Calphad*. 54 (2016) 35–53. doi:10.1016/j.calphad.2016.05.002.
- [27] J.M. Jones, L.I. Darvell, T.G. Bridgeman, M. Pourkashanian, A. Williams, An investigation of the thermal and catalytic behaviour of potassium in biomass combustion, *Proc. Combust. Inst.* 31 (2007) 1955–1963. doi:10.1016/j.proci.2006.07.093.
- [28] R. Malgorzata, Investigation of thermodynamic properties of alkali metals in oxide systems relevant to coal slags, OPUS3-IDN2331. (n.d.). <http://darwin.bth.rwth-aachen.de/opus3/volltexte/2008/2331/> (accessed August 20, 2018).
- [29] C. Mueller, M. Selenius, M. Theis, B.-J. Skrifvars, R. Backman, M. Hupa, H. Tran, Deposition behaviour of molten alkali-rich fly ashes—development of a submodel for CFD applications, *Proc. Combust. Inst.* 30 (2005) 2991–2998. doi:10.1016/j.proci.2004.08.116.
- [30] A.K. Biswas, M. Rudolfsson, M. Broström, K. Umeki, Effect of pelletizing conditions on combustion behaviour of single wood pellet, *Appl. Energy*. 119 (2014) 79–84. doi:10.1016/j.apenergy.2013.12.070.

List of Figures

Figure 1: Primary energy consumption increase since 1850 [1]	1
Figure 2: Principle of the DFB gasification system [9]	6
Figure 3: Melt- and coating induced agglomeration mechanism [13].....	13
Figure 4: Sub-processes of the bed agglomeration mechanism [16].....	14
Figure 5: Mechanism of the crack formation [17].....	15
Figure 6: ESEM image with inner and outer layer on olivine bed particle [18].....	16
Figure 7: Characteristic shapes of a test particle	17
Figure 8: Schematic of the bench scale FB reactor [20]	18
Figure 9: Pelletizer from company Cissonius with electrical power of 7.5kW	20
Figure 10: Wheat straw lignin before and after pelletizing	21
Figure 11: Vibration sieve from Fuchs Mühlen	23
Figure 12: Lab-scale FB reactor, schematic drawing and photograph [24].....	24
Figure 13: Bench-scale reactor, schematic drawing and photograph	25
Figure 14: Novel 100 kW DFB pilot-plant.....	27
Figure 15: Temperature profile of wheat straw combustion in the lab-scale reactor .	32
Figure 16: Pressure profile of wheat straw combustion in the lab-scale reactor	32
Figure 17: Wheat straw combustion - the agglomerates (left) and the bed material (right); 300 g of bed material.....	33
Figure 18: Wheat straw combustion - single large agglomerate; 50 g of bed material	33
Figure 19: Temperature profile of lignin combustion in the lab-scale reactor.....	34
Figure 20: Pressure profile of lignin combustion in the lab-scale reactor.....	34
Figure 21: Combustion of lignin in the lab-scale reactor - Sample of the ash (left) and the bed material (right).....	35
Figure 22: Temperature profile of wheat straw combustion in the bench-scale reactor	36
Figure 23: Pressure profile of wheat straw combustion in the bench-scale reactor ..	36
Figure 24: Composition profile of wheat straw combustion in the bench-scale reactor	37
Figure 25: Bench-scale reactor after experiment with wheat straw, deposit formation	37
Figure 26: Combustion of pelletized lignin in the bench-scale reactor.....	38
Figure 27: Combustion of non-pelletized lignin in the bench-scale reactor.....	38
Figure 28: Ash residues from the experiment with pelletized lignin	39
Figure 29: Ash residues from the experiment with non-pelletized lignin	39
Figure 30: Temperature profile of lignin gasification in the 100kW DFB pilot-plant...	40
Figure 31: Temperature profile of lignin gasification in the 100kW DFB pilot-plant during operation point OP 2.1	41
Figure 32: Temperature profile of lignin gasification in the 100kW DFB pilot-plant during operation point OP 2.2.....	41
Figure 33: Chemical equilibrium based on the fuel composition of wheat straw	43

Figure 34: Fraction of melting phase in the ash of wheat straw	43
Figure 35: Composition of the SLAG#1 of wheat straw	44
Figure 36: Composition of the SLAG#2 of wheat straw	44
Figure 37: Part of a ternary phase diagram of the $K_2O-CaO-SiO_2$ system with an eutectic point at 700 °C	45
Figure 38: Chemical equilibrium based on fuel composition for lignin	46
Figure 39: Composition of the SLAGA#1 for lignin	47
Figure 40: Composition of the SLAGA#2 for lignin	47
Figure 41: Fraction of melted phase in the lignin ash depending on temperature	48
Figure 42: Ternary diagram of the $Na_2O- Al_2O_3-SiO_2$ system with an eutectic point at 740 °C.....	49
Figure 43: Formation of the dense particle layer on the top of the bed.....	52
Figure 44: Formation of the softwood and the lignin ash	52
Figure 45: Crack formation on the non-pelletized lignin particle	53

List of Tables

Table 1: Main gasification reactions [8]	5
Table 2: Relative Lewis acid/base potential [12].....	9
Table 3: Secondary ash reactions [11]	9
Table 4: Tertiary ash reactions [12]	10
Table 5: Gas-phase reactions of alkali species (“M” stands for either K or Na).....	10
Table 6: Silication reactions of alkali species.....	11
Table 7: Comparison of the methods by Skrifvars et al. [19]	19
Table 8: Important parameters of wheat straw and lignin (d.b.-dry basis)	21
Table 9: XRF analysis of wheat straw and lignin ash	22
Table 10: Elemental analysis of wheat straw and lignin	22
Table 11: Minimal fluidization velocity and corresponding air volume flow at 20 and 850 °C	25
Table 12: Minimal fluidization velocity and corresponding air volume flow at 20 and 850 °C	26
Table 13: Ash composition of the ash residues from the experiment in the 100kW DFB pilot-plant (Ash residues) and from the fuel analysis (Feedstock ash)	42